# MODELS AND METHODS SUMMARY for the FEHM APPLICATION

**by**

**George A. Zyvoloski**
**Bruce A. Robinson**
**Zora V. Dash**
**Lynn L. Trease**

Modification date: 7/20/99

# TABLE OF CONTENTS

# LIST OF TABLES

# LIST OF FIGURES

# 1.0 PURPOSE

This Models and Methods Summary provides a detailed description of the mathematical models and numerical methods employed by the FEHM application.

# 2.0 DEFINITIONS AND ACRONYMS

## 2.1 Definitions

**FEHM**. Finite element heat and mass transfer code (Zyvoloski, et al. 1988).

**FEHMN**. YMP version of FEHM (Zyvoloski, et al. 1992).

## 2.2 Acronyms

**LANL**. Los Alamos National Laboratory.

**RTD**. Residence time distribution.

**RTTF**. Residence time transfer function.

**SOR**. Simultaneous over-relaxation.

**YMP**. Yucca Mountain Site Characterization Project.

# 3.0 REFERENCES

Birdsell, K. H., K. Campbell, K. G. Eggert, and B. J. Travis, "Simulation of Radionuclide Retardation at Yucca Mountain Using a Stochastic Mineralogical/Geochemical Model," *Proceedings of the First International Meeting on High Level Radioactive Waste Management*, Las Vegas, Nevada, April 8-12 (1990).

Brigham, W. E., "Mixing Equations in Short Laboratory Cores," *Soc. Pet. Eng. J.* **14**: 91-99 (1974).

Brownell, D. H., S. K. Garg, and J. W. Pritchett, "Computer Simulation of Geothermal Reservoirs," Paper SPE 5381, *Proceedings of the 45th California Regional Meeting of the Soc. Pet. Eng. of AIME*, Ventura, California (1975).

Bullivant, D. and G.A. Zyvoloski, "An Efficient Scheme for the Solution of Linear System Arising from Coupled Differential Equations," Los Alamos document, LA-UR-90-3187 (1990).

Case, C. M., *Physical Principles of Flow in Unsaturated Porous Media*, Clarendon Press, Oxford (1994).

Corey, A. T., "The Interrelation Between Gas and Oil Relative Permeabilities," *Prod. Mon.* **19**: 38-41 (1954).

Dalen, V., "Simplified Finite-Element Models for Reservoir Flow Problems," *Soc. Pet. Eng. J.* **19**: 333-343 (1979).

Engesgaard, P. and K. L. Kipp, "A Geochemical Model for Redox-controlled Movement of Mineral Fronts in Ground-water Flow Systems: A Case of NitrateRemoval by Oxidation of Pyrite," *Water Resour. Res.* **28**: 3308-3327 (1992).

Friedly, J. C., and J. Rubin, "Solute Transport with Multiple Equilibrium-Controlled or Kinetically Controlled Chemical Reactions," *Water Resour. Res.* **28(6)**: 1935-1953 (1992).

Fung, L. S. K., L. Buchanan, and R. Sharma, "Hybrid-CVFE Method for Flexible -Grid Reservoir Simulation," *Soc. Pet. Eng. J.* **19**: 188-199 (1994)

Gangi, A. F., “Variation of Whole and Fractured Porous Rock Permeability with Confining Pressure,” *Rock Mech. Sci. and Geomech. Abstr.* **15**: 249-157 (1978).

Harr, L., J. Gallagher, and G. S. Kell, *NBS/NRC Steam Tables, Thermodynamics, and Transport Properties and Computer Programs for Vapor and Liquid States of Water,* Hemisphere Press (1984).

Hinton, E., and D. R. J. Owen, *An Introduction to Finite Element Computations,* Pineridge Press, Swansea, Wales (1979).

Kinzelbach, W., W. Schafer, and J. Herzer, “Numerical Modeling of Natural and Enhanced Denitrification Processes in Aquifers,” *Water Resour. Res.,* **27**: 1123-1135 (1991).

Klavetter, E. A., and R. R. Peters, “Estimation of Hydrologic Properties of an Unsaturated Fractured Rock Mass,” Sandia Report SAND84-2642 (1986).

Lichtner, P. C., “Continuum Formulation of Multicomponent-multiphase Reactive Transport,” *Rev. in Mineralogy,* Vol. 34, Chapter 1, 1-81 ( 1996).

Lu, N., “A Semianalytical Method of Path Line Computation for Transient Finite-Difference Groundwater Flow Models,” *Water Resour. Res.* **30(8)**: 2449-2459 (1994).

Maloszewski, P., and A. Zuber, “On the Theory of Tracer Experiments in fissured Rocks with a Porous Matrix,” *J. Hydrol.* **79**: 333-358 (1985).

Mangold, D. C., and C. F. Tsang, “A Sumary of Subsurface Hydrological and Hydrochemical Models,” *Rev. Geophys.*, **29**: 51-79 (1991 ).

Mercer, J. W., and C. R. Faust, “Simulation of Water- and Vapor-Dominated Hydrothermal Reservoirs,” Paper SPE 5520, *Proceedings of the 50th Annual Fall Meeting of the Soc. Pet. Eng. of AIME,* Dallas, Texas (1975).

Moench, A. F., “Double-Porosity Models for a Fissured Groundwater Reservoir with Fracture Skin,” *Water Resour. Res.* **20(7)**: 831-846 (1984).

Neretnicks, I., “Diffusion in the Rock Matrix: An Important Factor in Radionuclide Migration?”, *J. Geophys. Res.* **85**(**B8**): 4379-4397 (1980).

Nitao, J., “Numerical Modeling of the Thermal and Hydrological Environment Around a Nuclear Waste Package Using the Equivalent Continuum Approximation: Horizontal Emplacement,” Lawrence Livermore National Laboratory Report UCID-21444 (1988).

Plummer, L. N., and E. Busenberg, “The Solubilities of Calcite, Argonite, and Vaterite in $CO_2$-$H_2O$ Solutions Between 0 and 90$^o$C, and an Evaluation of the Aqueous model for the System CaCO3-H2O,” *Geochim. et Cosmochim. Acta*, **46**: 1101 (1982).

Polzer, W. L., M. G. Rao, H. R. Fuentes, and R. J. Beckman, “Thermodynamically Derived Relationships Between the Modified Langmuir Isotherm and Experimental Parameters,” submitted to *Environmental Science and Technology* (1992).

Pruess, K., “TOUGH2 - A General-Purpose Numerical Simulator for Multiphase Fluid and Heat Flow,” Lawrence Berkeley Laboratory Report LBL-29400 (1991).

Reeves, M. (ed), “Review and Selection of Unsaturated Flow Models”, Intera Document B00000000-01425-2200-00001 Rev. 00, (1993).

Reimus, P. W., “The Use of Synthetic Colloids in Tracer Transport Experiments in Saturated Rock Fractures,” Ph.D. Thesis, The University of New Mexico, Albuquerque, New Mexico (1995).

Robinson, B., "Model and Methods Summary for the SORBEQ Application," Los Alamos document SORBEQ MMS, ECD-20 (1993).

Robinson, B. A., "A Strategy for Validating a Conceptual Model for Radionuclide Migration in the Saturated Zone Beneath Yucca Mountain," *Rad. Waste Manag. Envir. Rest.* **19**: 73-96 (1994).

Starr, R. C., R. W. Gillham, and E. A. Sudicky, "Experimental Investigation of Solute Transport in Stratified Porous Media 2. The Reactive Case," *Water Resour. Res.* **21(7)**: 1043-1050 (1985).

Steefel, C.I. and A.C. Lasaga, "A Coupled Model for Transport of Multiple Chemical Species and Kinetic Precipitation/dissolution Reactions with Application to Reactive Flow in Single Phase Hydrothermal Systems," *American Journal of Science*, **294**: 529-592 (1994).

Sychev, V. V., et al., *Thermodynamic Properties of Air*, Hemisphere Publishing Corp. (1988).

Tang, D. H., E. O. Frind, and E. A. Sudicky, "Contaminant Transport in Fractured Porous Media: Analytical Solution for a Single Fracture," *Water Resour. Res.* **17(3)**: 555-564 (1981).

Tebes-Stevens, C., A. J. Valocchi, J. M. VanBriesen, and B. E. Rittmann, "Multicomponent Transport with Coupled Geochemical and Microbiological Reactions: Model Description and Example Simulations," submitted to *J. Hyrol.* (1998).

Tompson, A. F. B., and L. W. Gelhar, "Numerical simulation of Solute Transport in Three-Dimensional, Randomly Heterogeneous Porous Media," *Water Resour. Res.*, 26, 10, 2541-2562 (1990).

van Genuchten, M. T., "A Closed Form Equation for Predicting Hydraulic Conductivity of Unsaturated Soils," *Soil Sci. Soc. Am. J.* **44**: 892-898 (1980).

Warren, J. E., and P. J. Root, "The Behavior of Naturally Fractured Reservoirs," *Soc. Pet. Eng. J.* **3**: 245-255 (1963).

Weeks, E. P., "Effect of Topography on Gas Flow in Unsaturated Fractured Rock: Concepts and Observations," *Proceedings of the American Geophysical Union Symposium on Flow and Transport in Unsaturated Fractured Rock*, D. Evans and T. Nicholson, Eds., Geophysical Monograph **42**: AGU (1987).

Wolery, T. J., "EQ3NR, A Computer Program for Geochemical Aqueous Speciation-Solubility Calculations: Theoretical Manual, User's Guide, and Related Documentation (Version 7.0)," Technical Report UCRL-MA-110662-PT-IV, Lawrence Livermore National Laboratory (1992).

Yeh, G. T., and V. S. Tripathi, "A Critical Evaluation of Recent Developments in Hydrogeochemical Transport Models of Reactive Multichemical Components," *Water Resour. Res.* **25**: 93-108 (1989).

Young, L. C., "A Finite Element Method for Reservoir Simulation," *Soc. Pet. Eng. J.* **21**: 115-128 (1981).

Zienkiewicz, O. C., *The Finite Element Method*, McGraw-Hill, London (1977).

Zienkiewicz, O. C., and C. J. Parekh, "Transient Field Problems - Two and Three Dimensional Analysis by Isoparametric Finite Elements," *Int. J. Numer. Methods Eng.* **2**: 61-70 (1973).

Zyvoloski, G., "Finite Element Methods for Geothermal Reservoir Simulation," *Int. J. Numer. Anal. Methods Geomech.* **7**: 75-86 (1983).

Zyvoloski, G. A., and Z. V. Dash, "Software Verification Report FEHMN Version 1.0," LA-UR-91-609 (1991).

Zyvoloski, G. A., Z. V. Dash, and S. Kelkar, "FEHMN 1.0: Finite Element Heat and Mass Transfer Code," LA-12062-MS, Rev. 1 (1992).

Zyvoloski, G. A., Z. V. Dash, and S. Kelkar, "FEHM: Finite Element Heat and Mass Transfer Code," LA-11224-MS (1988).

Zyvoloski, G. A., M. J. O'Sullivan, and D. E. Krol, "Finite Difference Techniques for Modeling Geothermal Reservoirs," *Int. J. Numer. Anal. Methods Geomech.* **3**, 355-366 (1979).

Zyvoloski, G. A., and B. A. Robinson, *GZSOLVE Application*, Los Alamos National Laboratory software documents ECD-97 (1995).

## 4.0 NOTATION

Variables used in derivation of the component and numerical model are enumerated in Table I with reference to the equations in which they appear.

**Table I. Nomenclature**

| | |
|---|---|
| General notation conventions | |
| $\tilde{A}$ | Approximation of A |
| $\overline{A}$ | Vector A |
| $[A]$ | Two dimensional array A |
| $\{A\}$ | One dimensional array/vector A |
| Subscripts | |
| *a* | Subscript denoting air properties |
| *b* | Subscript denoting biomass |
| *c* | Subscript denoting concentration |
| *cap* | Subscript denoting capillary values |
| *dry* | Subscript denoting value at 0 saturation |
| *e* | Subscript denoting energy |
| *f* | Subscript denoting fracture properties |
| *flow* | Subscript denoting properties of flowing fluid |
| *i, j, k* | Subscripts denoting nodal position (node indices) |
| *i* | Subscript denoting complex |
| *j, k, m* | Subscripts denoting component |
| *l* | Subscript denoting liquid properties |
| *lr* | Subscript denoting residual liquid |
| *m* | Subscript denoting mass or matrix property for dual porosity formulations |

* Units given in MLθT system of dimensions: mass [M], length [L], time [θ], temperature [T]

**Table I. Nomenclature (Continued)**

| | |
|---|---|
| *max* | Subscript denoting maximum value |
| *min* | Subscript denoting minimum value |
| *P* | Subscript denoting derivative with respect to pressure |
| *p* | Subscript denoting fluid phase |
| *p* | Subscript denoting precipitation |
| *r* | Subscript denoting rock properties |
| *ref* | Subscript denoting value at reference conditions |
| *S* | Subscript denoting derivative with respect to saturation |
| *s* | Subscript denoting slope of a linear relation |
| *sat* | Subscript denoting saturation dependence |
| *T* | Subscript denoting derivative with respect to temperature or temperature dependence |
| *v* | Subscript denoting vapor properties |
| *vr* | Subscript denoting residual vapor |
| *w* | Subscript denoting water properties |
| *x, y, z* | Subscripts denoting coordinate direction |
| η | Subscript denoting noncondensible gas |
| 0 | Subscript denoting initial value |
| *1, 2, . . ., m, m+1, . . ., n* | Subscripts denoting the specie or component (i.e., *n*th component) |
| Superscripts | |
| *UP* | Superscript denoting upstream-weighted value |
| *0, k, k+1* | Superscripts denoting iteration (i.e., *k*th iteration) |
| *n, n+1* | Superscripts denoting timestep (i.e., *n*th timestep) |
| Parameters | |
| A | Internode area projection for finite volume calculation ($L^2$) [Figure 3] |
| $[A]$ | Solution matrix for system of nonlinear equations [Equations (47) - (54), (64) - (72)] |
| $A_c$ | Concentration (solute) accumulation term $\left(\frac{\text{moles}}{L^3}\right)$ [Equations (36), (75), (76), (80)] |
| $A_e$ | Energy accumulation term $\left(\frac{M}{L\theta^2}\right)$ [Equations (4), (5), (10), (16), (26)] |

* Units given in MLθT system of dimensions: mass [M], length [L], time [θ], temperature [T]

**Table I. Nomenclature (Continued)**

| | |
|---|---|
| $A_m$ | Mass accumulation term $\left(\frac{M}{L^3}\right)$ [Equations (1), (2), (9), (25)] |
| $A_s$ | Reactive surface area ($L^2$) [Equation (93)] |
| $A_\eta$ | Noncondensible gas accumulation term $\left(\frac{M}{L^3}\right)$ [Equations (19), (20), (27)] |
| $a_{ij}$ | Stoichiometric coefficients used in reaction rate model [Equations (79), (85), (87)] |
| $a$ | Air conservation variable [Equations (50), (51)] |
| $b$ | First order microbial decay coefficient [Equation (90)] |
| $\{b\}$ | Residual vector, right hand side (forcing function) for system of linear equations [Equations (46), (64) - (72)] |
| $C$ | Concentration (solute) $\left(\frac{\text{moles}}{M}\right)$ [Equations (36), (37), (39), (73) - (76), (78) - (82), (85), (87), (93), (106), (109), (110),Table II] |
| $\hat{C}$ | Chemical formula for aqueous comonent [Equation (85)] |
| $\hat{C}$ | Normalized concentration [Equations (99), (100)] |
| $[\hat{C}]$ | Capacitance matrix [Equations (25), (26), (27), (32), (36)] |
| $c$ | Compressibility $\left(\frac{L\theta^2}{M}\right)$ [Equation (147)] |
| $c$ | Concentration $\left(\frac{\text{moles}}{M}\right)$ [Equations (79), (86) - (88), (91), (92)] |
| $c_p$ | Heat capacity/Specific heat $\left(\frac{L^2}{\theta^2 T}\right)$ [page 21, Equations (130), (131)] |
| $D_{AB}$ | Solute diffusion coefficient $\left(\frac{L^2}{\theta}\right)$ [Equation (77)] |
| $D_{cl}$ | Combination of molecular diffusion and dispersivity $\left(\frac{L^2}{\theta}\right)$ [Equation (77)] |
| $D_{va}$ | Air water diffusivity $\left(\frac{L^2}{\theta}\right)$ [Equations (20), (21), (27), (30), (35)] |
| $D_c$ | Dispersion coefficient for tracer $\left(\frac{L^2}{\theta}\right)$ [Equations (36), (38), (76), (80)] |
| $D_e$ | Energy transmissibility term $\left(\frac{L^2}{\theta}\right)$ [Equations (10), (12), (29), (34)] |
| $D_{eff}$ | Effective dispersion coefficient of a solute [Equation (96)] |

* Units given in MLθT system of dimensions: mass [M], length [L], time [θ], temperature [T]

**Table I. Nomenclature (Continued)**

| | |
|---|---|
| $D_m$ | Mass transmissibility term $(\theta)$ [Equations (9), (11), (12), (20), (22), (23), (28), (33), (35), (37), (39), (76)] |
| d | Internode distance for finite volume calculation (L) [Figure 3] |
| $E$ | Young's modulus $\left(\frac{ML}{\theta^2}\right)$ [Equation (78)] |
| $\{F\}$ | Equation residuals [Equations (25), (26), (27), (36), (42) - (54)] |
| $\|F\|$ | $l^2$ norm of residuals (square root of the sum of the residuals squared) [Equations (44), (45)] |
| $\left(\frac{\partial\{F\}}{\partial\{x\}^k}\right)$ | Jacobian matrix for nonlinear system [Equation (43)] |
| $\overline{f_c}$ | Flux vector for concentration equations $\left(\frac{\text{moles}}{L^2\theta}\right)$ [Equations (73), (80)] |
| $\overline{f_e}$ | Flux vector for energy equation $\left(\frac{M}{\theta^3}\right)$ [Equations (4), (6)] |
| $\overline{f_m}$ | Flux vector for mass equation $\left(\frac{M}{L^2\theta}\right)$ [Equations (1), (3)] |
| $\overline{f_\eta}$ | Flux vector for noncondensible gas equation $\left(\frac{M}{L^2\theta}\right)$ [Equation (17)] |
| $f(t)$ | Function at time $t$ [Equation (24)] |
| $f'(t)$ | Derivative of $f$ with respect to time [Equation (24)] |
| $G_k$ | Vapor concentration [Equations (83), (107), (109)] |
| $\{G\}$ | Gravity term coefficients [Equations (25), (26), (27), (33) - (36), (39)] |
| $g$ | Acceleration of gravity $\left(\frac{L}{\theta^2}\right)$ [Equations (9), (10), (20), (22), (23), (25), (26), (27), (36), (76)] |
| $\bar{g}$ | $g$ times the unit vector in the gravitational (z) direction [Equations (7), (8)] |
| $h$ | Enthalpy $\left(\frac{L^2}{\theta^2}\right)$ [Equations (6), (12), (13), (62), (63), (130), (132), (133)] |
| $I_m$ | Mass flow impedance $\left(\frac{\theta}{L^2}\right)$ [Equation (40)] |
| $I_e$ | Heat flow impedance $\left(\frac{M}{L^3\theta T}\right)$ [Equation (41)] |

* Units given in ML$\theta$T system of dimensions: mass [M], length [L], time [$\theta$], temperature [T]

**Table I. Nomenclature (Continued)**

| | |
|---|---|
| $K$ | Thermal conductivity $\left(\frac{ML}{T\theta^3}\right)$ [Equations (6), (16), (26), (31), (151), (152), page 26] |
| $K_A, K_S$ | Monod half-maximum-rate concentrations [Equation (89)] |
| $K_D$ | Distribution coefficient [Equation (88)] |
| $K_H$ | Henry's law constant $\left(\frac{L\theta^2}{M}\right)$ [Equation (135)] |
| $K_d$ | Retardation coefficient (linear adsorption) [Table II] |
| $K_i$ | Equilibrium formation constant [Equations (86), (87)] |
| $K_{sp}$ | Solubility product [Equation (93)] |
| $k$ | Intrinsic rock permeability $(L^2)$ [Equations (7), (8), (11), (61), (62), (63), (150)] |
| $k_+$ | Rate constant [Equation (93)] |
| $k_f$, $k_r$ | Forward and reverse reaction rate constants [Equations (111) - (113)] |
| $k_m$ | Mass transfer coefficient [Equation (88)] |
| $k_{Rn}$ | Radioactive decay rate constant [Equation (105)] |
| $L$ | Flow path length (m) |
| $L_f, L_{f0}, L_{f1}, L_{f2}$ | Length scales used in dual porosity and double porosity / double permeability problems [Equations (56), (58), (59), (60), Figure 4] |
| $L_l$ | Advection dispersion operator [Equations (81) - (83), (106), (107)] |
| $M_f$ | Fluid mass in a cell (kg) [Equation (94)] |
| $M_m$ | Immobile concentration (mass solute per mass rock matrix) [Equation (84), (108), (109)] |
| $m$ | Concentration $\left(\frac{\text{moles}}{M}\right)$ [Equations (88) - (91)] |
| $m$ | Exponent used in Gangi stress model [Equation (148)] |
| $\dot{m}_{out}$ | Outlet mass flow rate from one cell to another [Equation (94)] |
| $[N]$ | Finite element shape function [page 25, Equations (28) - (34), (37) - (39)] |
| $N_c$ | Number of aqueous components [Equations (79), (80), (85)-(87), (92)] |
| $N_{im}$ | Number of immobile components [Equation (84) |
| $N_n$ | Number of spatial grid points [page 44] |
| $N_v$ | Number of vapor components [Equation (83) |
| $N_x$ | Number of aqueous complexes [Equations (79), (87)] |

* Units given in MLθT system of dimensions: mass [M], length [L], time [θ], temperature [T]

**Table I. Nomenclature (Continued)**

| | |
|---|---|
| $n$ | Experimental parameter used in van Genuchten relative permeability and capillary pressure models [page 68, page 69] |
| $P$ | Pressure $\left(\frac{M}{L\theta^2}\right)$ [Equations (7) - (10), (20), (22), (23), (25), (26), (27), (36), (40), (47) - (54), (61), (62), (63), (76), (121) - (124), (128), (135), (144) - (147), (149)] |
| $P_c$ | Closure stress for use in Gangi stress model (ML) [Equations (148), (149)] |
| $Pe$ | Peclet number for dispersion [Equations (99) and (100)] |
| $Q_p$ | Solubility product {Equations (92), (93)] |
| $q_c$ | Concentration source term $\left(\frac{\text{moles}}{L^3\theta}\right)$ [Equations(36), (74), (76)] |
| $q_e$ | Energy source term $\left(\frac{M}{L\theta^3}\right)$ [Equations (4), (10), (13), (16), (26), (41)] |
| $q_{fm}$ | Solute flux term from fracture to matrix in particle tracking model development [Equation (102)] |
| $q_m$ | Mass source term $\left(\frac{M}{L^3\theta}\right)$ [Equations (1), (9), (14), (22), (23), (25), (40), (89)] |
| $q_\eta$ | Noncondensible gas source term $\left(\frac{M}{L^3\theta}\right)$ [Equations (18), (20), (27)] |
| $R$ | Kinetic reaction source-sink term [Equations (80), (82)-(84), (88) - (90), (106) - (110)] |
| $R$ | Universal gas constant (8.314 kJ/mol-K) [Equation (127)] |
| $R_f$ | Sorption retardation factor [Equation (95)] |
| $R_p$ | Relative permeability [Equations (7), (8), (11), (15), (138) - (143)] |
| $r, r_b$ | Parameters used in nonlinear adsorption model (Langmuir) [Table II] |
| $S$ | Saturation [Equations (2), (5), (19), (22), (23), (53) - (54), (80), (138) - (145)] |
| $T$ | Temperature (T) [Equations (6), (16), (41), (47), (48), (50) - (52), (121) - (124), (128), (130), (131), (149)] |
| $[T]$ | Stiffness matrix [Equations (25) - (29), (36), (37)] |
| $T_{ff1}, T_{f1f2}$ | Transfer terms in dual porosity solution [Equations (59) - (63)] |
| $t$ | Time (θ) [Equations (1), (4), (9), (10), (16), (20) - (27), (36), (76), (106) - (108)] |
| $u$ | Internal energy $\left(\frac{L^2}{\theta^2}\right)$ [Equation (5)] |
| $V$ | Integral volume [Equations (28) - (34), (37) - (39)] |

* Units given in MLθT system of dimensions: mass [M], length [L], time [θ], temperature [T]

**Table I. Nomenclature (Continued)**

| | |
|---|---|
| $V_f$ | Volume fraction for fractures in a dual porosity and double porosity / double permeability problems [Equations (55) - (58)] |
| $V_{f0}$, $V_{f1}$, $V_{f2}$ | Volume fractions for the matrix volumes used in dual porosity and double porosity / double permeability problems [Equations (55) - (58)] |
| $V_T$ | Total volume of computational cell ($L^3$) [[Equation (59), (60)] |
| $v$ | Superficial velocity in one-dimensional model used in particle tracking model development [Equation (96)] |
| $\bar{v}$ | Velocity vector $\left(\frac{L}{\theta}\right)$ [Equations (3), (6) - (8), (17)] |
| $v_{l,x}$ | Darcy velocity of liquid phase, x-direction [Equation (77)] |
| $w$ | Weighting factor for time discretization [Equation (24)] |
| $X$ | Pressure or temperature variable in rational function approximation for saturation equations [Equations (125), (126)] |
| $\hat{X}_i$ | Chemical formula for aqueous complex [Equation (85), (86)] |
| $\{x\}$ | Solution vector, [Equations (42), (43), (46), (64) - (72)] |
| $\hat{x}$ | Normalized distance along flow path [Equation (99)] |
| $Y$ | Microbial yield coeeficient [Equation (90)] |
| $Y$ | Polynomial in numerator of rational function approximation [Equations (121) - (126)] |
| $Z$ | Polynomial in denominator of rational function approximation [Equations (121) - (126)] |
| $z$ | Coordinate oriented in the direction of gravity [Equations (9), (10), (20), (33), (34), (39), (76)] |
| $\alpha$ | Coefficient of thermal expansion $\left(\frac{1}{T}\right)$ [Equation (149)] |
| $\alpha_1$, $\alpha_2$ | Coefficients used in sorption models [Equation (78), Table II] |
| $\alpha_a$ | Aquifer compressibility |
| $\alpha_d$ | Dispersivity of solute in transport calculations $(L)$ |
| $\alpha_G$ | Experimental parameter used in van Genuchten capillary pressure model [page 69] |
| $\beta$ | Exponent used in sorption models [Equation (78), Table II] |
| $\gamma$ | Activity coefficient for aqueous component [Equation (86)] |
| $\gamma_{rxn}$ | Fractional approach to equilibrium computed at an iteration in the reactive transport model [Equation (94)] |
| $\gamma_{tol}$ | Fractional approach to equilibrium specified for an equilibrium reaction [Equation (94)] |
| $\varepsilon$ | Tolerance taken for solution scheme [Equation (45)] |

* Units given in MLθT system of dimensions: mass [M], length [L], time [θ], temperature [T]

**Table I. Nomenclature (Continued)**

| | |
|---|---|
| $\eta$ | Mass fraction of air [Equations (2), (3), (9), (17) - (20), (27), (35), (132) - (136)] |
| $\theta$ | Exponent used in the air/water diffusion model [Equation (21)] |
| $\hat{\theta}$ | Normalized time [Equations (99)and (100)] |
| $\Lambda$ | Parameter used in nonlinear adsorption model (Freundlich, modified Freundlich) [Table II] |
| $\lambda$ | Parameter used in van Genuchten relative permeability and capillary pressure models [Equation (142), page 69] |
| $\mu$ | Viscosity $\left(\frac{M}{L\theta}\right)$ [Equations (7), (8), (11), (15), (61), (62), (63), (136), (137)] |
| $\mu_p$ | Stoichiometric coefficients used in reaction rate model [Equations (91) - (93)] |
| $\nu$ | Fractional vapor flow parameter [Equations (14), (15)] |
| $\rho$ | Density $\left(\frac{M}{L^3}\right)$ [Equations (3), (5), (7) - (11), (15), (17), (19) -(23), (61), (62), (63), (76), (80), (128), (129), (134) ] |
| $\sigma$ | *In situ* stress $\left(\frac{ML}{\theta^2}\right)$ [Equation (149)] |
| $\tau$ | Tortuosity factor in the air/water diffusion model [Equation (21)] |
| $\tau_{age}$ | Particle age since entering the model domain [Equation (105)] |
| $\tau_f$ | Fluid residence time in a cell (s) [Equation (94)] |
| $\tau_{part}$ | Particle residence time in a cell (s) [Equation (94)] |
| $\tau_{1/2}$ | Radioactive decay half-life |
| $\phi$ | Porosity [Equations (2), (5), (19), (21) - (23), (80), (147), (148), (150)] |
| $\phi_{mat}$ | Matrix porosity in particle tracking model [Equation (102)] |
| $\Omega$ | Flow domain of the model [Equations (28) - (34), (37) - (39)] |

* Units given in ML$\theta$T system of dimensions: mass [M], length [L], time [$\theta$], temperature [T]

# 5.0 STATEMENT AND DESCRIPTION OF THE PROBLEM

The primary use of the FEHM application will be to assist in the understanding of flow fields and mass transport in the saturated and unsaturated zones below the potential Yucca Mountain repository. Studies in the saturated zone are prescribed in YMP-LANL-SP-8.3.1.2.3.1.7 (the C-Wells project) and include use of the FEHM code to design and analyze tracer tests (reactive and non-reactive) to characterize the flow field below Yucca Mountain. Studies in the unsaturated zone are prescribed in YMP-LANL-SP-8.3.1.3.7.1 and include the study of coupled processes (multicomponent flow and natural convection).

Yucca Mountain is extremely complex both hydrologically and geologically. The computer codes that are used to model flow must be able to describe that complexity.

For example, the flow at Yucca Mountain, in both the saturated and unsaturated zones is dominated by fracture and fault flow in many areas. With permeation to and from faults and fractures, the flow is inherently three-dimensional (3-D). Birdsell, et al. (1990) presented calculations showing the importance of 3-D flow at Yucca Mountain. Coupled heat and mass transport occurs in both the unsaturated and saturated zones. In the near field region surrounding the repository, the coupled flow effects dominate the fluid behavior. Here boiling, dryout, and condensation can occur (Nitao, 1988). In the far field unsaturated zone, Weeks (1987) has described natural convection that occurs through Yucca Mountain due to seasonal temperature changes. Heat and mass transfer are also important in matching saturated zone models to temperature logs and pressure tests and in modeling enhanced convection from repository heating.

The transport processes at Yucca Mountain are very complex. Various adsorption mechanisms ranging from simple linear relations to nonlinear isotherms must be incorporated in the transport models. Multiple interacting chemical species must be modeled so that this structure can represent radioactive decay with daughter products and coupled geochemical transport.

# 6.0 STRUCTURE OF THE SYSTEM MODEL

The sub-models that make up the overall transport model are:

Flow and Energy Transport Equations for simulation of processes within porous and permeable media which include:

- Heat conduction only;
- Heat and mass transfer with pressure and temperature dependent properties, relative permeabilities and capillary pressures;
- Isothermal air-water transport; and
- Heat and mass transfer with noncondensible gas.

Dual Porosity and Double Porosity / Double Permeability Formulation for problems dominated by fracture flow.

Solute Transport Models, including:

- A reactive transport model that simulates transport of multiple solutes with chemical reaction; and
- A particle tracking model.

Constitutive Relationships for pressure and temperature dependent fluid/air/gas properties, relative permeabilities and capillary pressures, stress dependencies, and reactive and sorbing solutes which encompass:

- Thermodynamic equations;
- Air and Air/Water Vapor Mixtures;
- Equation of State Models;
- Relative Permeability and Capillary Pressure Functions;
- Stress Dependent Properties; and
- Variable Thermal Conductivity.

# 7.0 GENERAL NUMERICAL PROCEDURE

The numerical solution strategy for FEHM is shown in Figure 1.

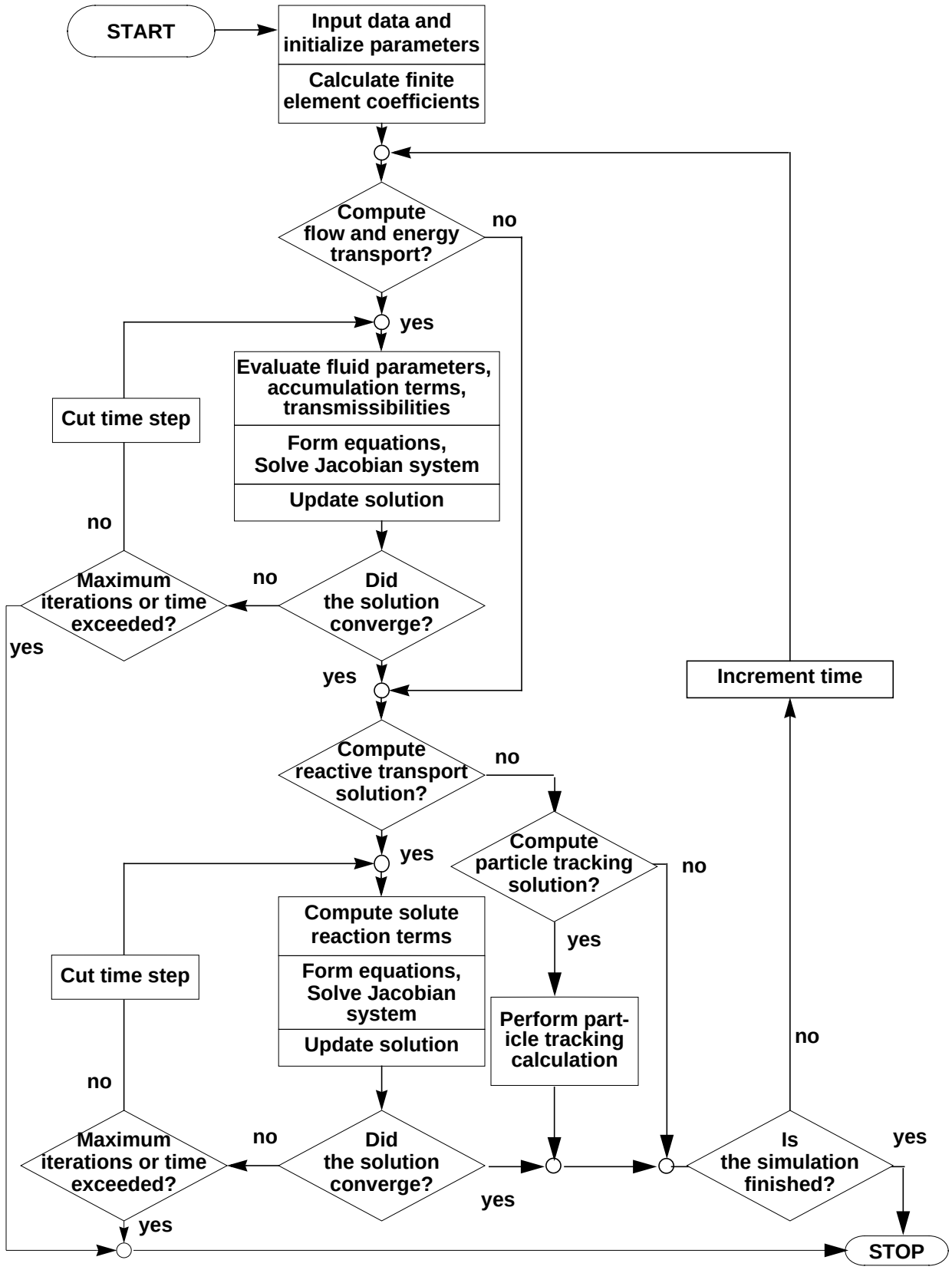


**Figure 1. Simplified diagram of code flow in the FEHM application.**

# 8.0 COMPONENT MODELS

## 8.1 Flow and Energy Transport

### 8.1.1 Purpose

The purpose of this model is to simulate heat conduction, heat and mass transfer for multiphase flow within porous and permeable media, and noncondensible gas flow within porous and permeable media.

For heat conduction the input to the model consists of an initial description of the media (rock) properties and state. The output consists of a final media state.

For heat and mass transfer the input to the model consists of an initial description of the fluid state as well as media properties. The output consists of the final fluid and media states.

For noncondensible gas flow, in addition to the initial media properties and fluid state, the description of the initial state of gas is required. The output consists of the final state of gas in addition to that described for the previous components.

### 8.1.2 Assumptions and Limitations

The major assumptions are those associated with Darcy's law for fluid flow. This restricts the velocity of fluid flow to be very slow. The exact quantification of the values is best addressed in the associated validation report. Another assumption is thermal equilibrium between fluid and rock (locally). This is usually an excellent assumption as the thermal wave for rocks travels on the order of $10^{-3}$ m/s, $10^{-3}$ m is the upper limit of the pore size and fluid velocities are of the order of $10^{-5}$ m/s.

Other assumptions include an immovable rock phase and negligible viscous heating. The assumptions associated with flow are discussed in Brownell, et al. (1975)

### 8.1.3 Derivation

Because the derivation of the governing equations is analogous for heat conduction, heat and mass transfer for multiphase flow within porous and permeable media, noncondensible gas flow within porous and permeable media, and transport of multiple solutes within porous and permeable media, only the heat and mass derivation will be presented.

Detailed derivations of the governing equations for two-phase flow including heat transfer have been presented by several investigators (e.g., Mercer and Faust, 1975, and Brownell, et al. 1975), therefore only a brief development will be presented. The notation used is given in Table I.

Conservation of mass for water is expressed by the equation

$$\frac{\partial A_m}{\partial t} + \overline{\nabla} \cdot \overline{f_m} + q_m = 0, \tag{1}$$

where the mass per unit volume, $A_m$, is given by

$$A_m = \phi(S_v \rho_v (1 - \eta_v) + S_l \rho_l (1 - \eta_l)) \tag{2}$$

and the mass flux, $\overline{f_m}$, is given by

$$\overline{f_m} = (1-\eta_v)\rho_v\overline{v_v} + (1-\eta_l)\rho_l\overline{v_l} \ . \tag{3}$$

Here $\phi$ is the porosity of the matrix, $S$ is saturation, $\rho$ is density, $\eta$ is the concentration of the noncondensible gas and is expressed as a fraction of the total mass, and $\bar{v}$ is velocity with the subscripts $v$ and $l$ indicating quantities for the vapor phase and the liquid phase, respectively. Source and sink terms (such as bores, reinjection wells, or groundwater recharge) are represented by the term $q_m$.

Conservation of fluid-rock energy is expressed by the equation

$$\frac{\partial A_e}{\partial t} + \bar{\nabla}\cdot\overline{f_e} + q_e = 0, \tag{4}$$

where the energy per unit volume, $A_e$, is given by

$$A_e = (1-\phi)\rho_r u_r + \phi(S_v\rho_v u_v + S_l\rho_l u_l) \tag{5}$$

with $u_r = c_{pr}T$, and the energy flux, $\overline{f_e}$, is given by

$$\overline{f_e} = \rho_v h_v\overline{v_v} + \rho_l h_l\overline{v_l} - K\bar{\nabla}T \ . \tag{6}$$

Here the subscript $r$ refers to the rock matrix; $u_r$, $u_v$, and $u_l$ are specific internal energies; $c_{pr}$ is the specific heat; $h_v$ and $h_l$ are specific enthalpies; $K$ is an effective thermal conductivity; $T$ is the temperature; and $q_e$ is the energy contributed from sources and sinks.

To complete the governing equations it is assumed that Darcy's Law applies to the movement of each phase:

$$\overline{v_v} = -\frac{kR_v}{\mu_v}(\bar{\nabla}P_v - \rho_v\bar{g}) \tag{7}$$

and

$$\overline{v_l} = -\frac{kR_l}{\mu_l}(\bar{\nabla}P_l - \rho_l\bar{g}) \ . \tag{8}$$

Here $k$ is the permeability, $R_v$ and $R_l$ are the relative permeabilities, $\mu_v$ and $\mu_l$ are viscosities, $P_v$ and $P_l$ the phase pressures, and $g$ represents the acceleration due to gravity (the phase pressures are related by $P_v = P_l + P_{cap}$, where $P_{cap}$ is the capillary pressure). For simplicity, the

equations are shown for an isotropic medium, though this restriction does not exist in the computer code.

Using Darcy's Law the basic conservation Equations (1) through (4) can be combined

$$-\overline{\nabla}\cdot((1-\eta_v)D_{mv}\overline{\nabla}P_v)-\overline{\nabla}\cdot((1-\eta_l)D_{ml}\overline{\nabla}P_l)+q_m+\frac{\partial}{\partial z}g((1-\eta_v)D_{mv}\rho_v+(1-\eta_l)D_{ml}\rho_l)+\frac{\partial A_m}{\partial t}=0 \quad (9)$$

and

$$-\overline{\nabla}\cdot(D_{ev}\overline{\nabla}P_v)-\overline{\nabla}\cdot(D_{el}\overline{\nabla}P_l)-\overline{\nabla}\cdot(K\overline{\nabla}T)+q_e+\frac{\partial}{\partial z}g(D_{ev}\rho_v+D_{el}\rho_l)+\frac{\partial A_e}{\partial t}=0 \quad (10)$$

where $z$ is oriented in the direction of gravity. Here the transmissibilities are given by

$$D_{mv}=\frac{kR_v\rho_v}{\mu_v},\ D_{ml}=\frac{kR_l\rho_l}{\mu_l} \quad (11)$$

and

$$D_{ev}=h_vD_{mv},\ D_{el}=h_lD_{ml}\ . \quad (12)$$

The source and sink terms in Equations (1) and (4) arise from bores, and if the total mass withdrawal, $q_m$, for each bore is specified, then the energy withdrawal, $q_e$, is determined as follows:

$$q_e=q_vh_v+q_lh_l \quad (13)$$

where

$$q_v=\nu q_m,\ q_l=(1-\nu)q_m \quad (14)$$

and

$$\nu=\frac{1}{1+\frac{\rho_lR_l\mu_v}{\rho_vR_v\mu_l}}\ . \quad (15)$$

The form of Equation (15) shows how important the relative permeability ratio $R_l/R_v$ is in controlling the discharge composition. Other source/sink terms arise from implementation of boundary conditions. These include specified pressure and temperatures and are discussed in Section 8.1.6, "Derivation of Numerical Model" subsection "Boundary Conditions". The

relative permeability and capillary pressure functions are summarized in Section 8.4, “Constitutive Relationships”.

The final form of the pure heat conduction equation is easily obtained from Equation (10) when all convective terms are eliminated:

$$-\bar{\nabla} \cdot (K\bar{\nabla}T) + q_e + \frac{\partial A_e}{\partial t} = 0 \ . \tag{16}$$

The mass flux, $\overline{f_\eta}$, source (or sink) strength, $q_\eta$, and accumulation term, $A_\eta$, are defined as follows for the noncondensible gas conservation equation:

$$\overline{f_\eta} = \eta_v \rho_v \overline{v_v} + \eta_l \rho_l \overline{v_l} \ , \tag{17}$$

$$q_\eta = \eta_v q_v + \eta_l q_l \ , \tag{18}$$

$$A_\eta = \phi(\eta_v S_v \rho_v + \eta_l S_l \rho_l) \ . \tag{19}$$

The noncondensible gas conservation equation is

$$-\bar{\nabla} \cdot (\eta_v D_{mv} \bar{\nabla} P_v) - \bar{\nabla} \cdot (\eta_l D_{ml} \bar{\nabla} P_l) - \bar{\nabla} \cdot (D_{va} \bar{\nabla} \eta_v) + q_\eta + \frac{\partial}{\partial z} g(\eta_v D_{mv} \rho_v + \eta_l D_{ml} \rho_l) + \frac{\partial A_\eta}{\partial t} = 0 \ . \tag{20}$$

Here $\eta$ is the concentration of the noncondensible gas and is expressed as a fraction of the total mass. As with the water balance equations, source/sink terms are used to implement boundary conditions. The reader is referred to Section 8.1.6, “Derivation of Numerical Model” subsection “Boundary Conditions” for details.

The air water diffusivity (Pruess, 1991) is given by

$$D_{va} = \tau \phi S_v D_{va}^0 \rho_v \frac{0.101325}{P} \left[ \frac{T + 273.15}{273.15} \right]^\theta \tag{21}$$

where $\tau$ is the tortuosity factor and $D_{va}^0$ is the value of $D_{va}$ at standard conditions. Within FEHM the value of $D_{va}$ is set to $2.4*10^{-5}$ $m^2/s$, $\theta$ is set to 2.334, and the tortuosity factor is an input parameter.

The Equations (9), (10), (16), and (20) represent the model equations for fluid and energy transport in the computer code FEHM. It should be noted that Equation (9) also represents pure water with $\eta$ set to 0.

For situations in which heat effects are minimal, the model can be simplified. The isothermal air-water two phase system in FEHM is represented somewhat differently than the nonisothermal system defined above. Here the liquid phase is pure water and the vapor phase is pure air.

The component mass balance equations are then also phase balance equations:

$$\frac{\partial}{\partial t}(\phi \rho_l S_l) - \bar{\nabla} \cdot (D_{ml} \bar{\nabla} P_l) + q_{ml} + \frac{\partial}{\partial z} g(D_{ml} \rho_l) = 0 \ , \tag{22}$$

$$\frac{\partial}{\partial t}(\phi \rho_v S_v) - \bar{\nabla} \cdot (D_{mv} \bar{\nabla} P_v) + q_{mv} + \frac{\partial}{\partial z} g(D_{mv} \rho_v) = 0 \ . \tag{23}$$

where Equation (22) is the water balance equation and Equation (23) refers to the conservation of air. Here the subscript $l$ refers to the liquid water properties and $v$ refers to air properties. One option in the model is to solve Equations (22) and (23) as a full two-phase flow problem. A further simplification can be made in which the air pressure is assumed to be constant. This leads to an equation which is similar to the Richard's equation for unsaturated flow. The method reduces to using only Equation (22). The method is described further in Section 8.1.6 subsection “Reduced Degree of Freedom Algorithms”.

### 8.1.4 Applications

The component model described above may be used to model the flow of air, water, water vapor, and heat in a porous medium. The validity of the model is dependent on the validity of the equations described in Section 8.1.3. The flow of both air and water must be sufficiently small at all possible flow rates so that the above described equations will be valid. This is believed to be the case at Yucca Mountain. Of more concern is the accuracy of the required input and the numerical precision to which these equations are solved.

For the flow equations, the saturated permeabilities, porosities, and fracture permeabilities and volumes of hydrogeologic units are required. In addition, the relative permeability and capillary pressure functions are also required. Historically this information has been difficult to obtain. It is important to note that the capillary pressure at low liquid saturations is very important to the validity of the calculations but is not available in regions near the residual saturations.

The issue of numerical accuracy is extremely important to the usefulness of the results. The accuracy may be evaluated by solving the same problem using different size grids and evaluating the change in the solution.

### 8.1.5 Numerical Method Type

The primary numerical method used in FEHM is the Finite Element Method. The reader is referred to Zienkiewicz (1977) for an excellent account of the method. The summary of the numerics in FEHM given in Section 8.1.6 assumes a basic knowledge of the numerical solution of Partial Differential Equations. In addition a working knowledge of the Finite Element method is helpful.

### 8.1.6 Derivation of Numerical Model

**Discretization**: The time derivatives in Equations (9), (10), (16), (20), and (76) are discretized using the standard first order method (Hinton and Owen, 1979) given by

$$f(t^{n+1}) = f(t^n) + \Delta t[w f''(t^{n+1}) + (1-w) f''(t^n)] \quad (24)$$

where $f(t^{n+1})$ is the desired function at time $t^{n+1}$, $f(t^n)$ is the known value of $f$ at time $t^n$, $\Delta t$ is the time step, $f''$ is the derivative of $f$ with respect to time and $w$ is a weighting factor. For $w = 1$, the scheme is fully implicit (backward Euler) and for $w = 0$, the scheme is fully explicit (forward Euler).

The space derivatives in the governing equations are discretized using the finite element formulation. The finite element equations are generated using the Galerkin formulation. For a detailed presentation of the finite element method the reader is referred to Zienkiewicz (1977). In this method the flow domain, $\Omega$, is assumed to be divided into finite elements; and variables $P$, $T$, and $\eta$, along with the accumulation terms $A_m$, $A_e$, and $A_\eta$ are interpolated in each element: $P_v = [N]\{P_v\}$, $P_l = [N]\{P_l\}$, $T = [N]\{T\}$, $\eta_v = [N]\{\eta_v\}$, $A_m = [N]\{A_m\}$, $A_e = [N]\{A_e\}$, and $A_\eta = [N]\{A_\eta\}$ where $[N]$ is the shape function.

These approximations are introduced in Equations (9), (10), (16), and (20), and the Galerkin formulation (described by Zienkiewicz and Parekh, 1973) is applied. The following equations are derived:

$$[T_{m,v}]\{P_v\} + [T_{m,l}]\{P_l\} + [\hat{C}]\left\{\frac{\partial A_m}{\partial t}\right\} + \{q_m\} - g\{G_{m,v}\} - g\{G_{m,l}\} = \{F_m\}, \quad (25)$$

$$[T_{e,v}]\{P_v\} + [T_{e,l}]\{P_l\} + [K]\{T\} + [\hat{C}]\left\{\frac{\partial A_e}{\partial t}\right\} + \{q_e\} - g\{G_{e,v}\} - g\{G_{e,l}\} = \{F_e\} \quad (26)$$

and

$$[T_{\eta,v}]\{P_v\} + [T_{\eta,l}]\{P_l\} + [D_{va}]\{\eta_v\} + [\hat{C}]\left\{\frac{\partial A_\eta}{\partial t}\right\} + \{q_\eta\} - g\{G_{\eta,v}\} - g\{G_{\eta,l}\} = \{F_\eta\} \quad (27)$$

where

$$T_{mij} = \int_\Omega \bar{\nabla} N_i \cdot D_m^{UP} \bar{\nabla} N_j \, dV, \quad (28)$$

$$T_{eij} = \int_{\Omega} \bar{\nabla} N_i \cdot D_e^{UP} \bar{\nabla} N_j \, dV \,, \tag{29}$$

$$T_{\eta ij} = \int_{\Omega} \bar{\nabla} N_i \cdot D_m \eta^{UP} \bar{\nabla} N_j \, dV \,, \tag{30}$$

$$\zeta_{ij} = \int_{\Omega} \bar{\nabla} N_i \cdot \hat{K} \, \bar{\nabla} N_j \, d\forall \,, \tag{31}$$

$$\hat{C}_{ij} = \int_{\Omega} N_i N_j \, dV \,, \tag{32}$$

$$G_{mi} = \int_{\Omega} \frac{\partial N_i}{\partial z} N_j D_m^{UP} \rho_m \, dV \,, \tag{33}$$

$$G_{ei} = \int_{\Omega} \frac{\partial N_i}{\partial z} N_j D_e^{UP} \rho_e \, dV \,, \tag{34}$$

and

$$G_{\eta i} = \int_{\Omega} \frac{\partial N_i}{\partial z} N_j D_m \eta^{UP} \rho_e \, dV \,. \tag{35}$$

In the above equations $\hat{K} = \frac{2K_i K_j}{K_i + K_j}$, and the $D^{UP}$ terms indicate an upstream-weighted transmissibility (Dalen, 1979). This technique has worked well in the low-order elements (3-node triangle, 4-node quadrilateral), where the schemes resemble difference techniques. The upstream weighting is determined by evaluating the internode flux for the nodes $i$ and $j$. The shape function coefficients are generated in a unique way that requires the integrations in Equations (33), (34), and (35) to be performed only once and the nonlinear coefficients to be separated from this integration. The reader is referred to Zyvoloski (1983) for more details.

The integration schemes available in FEHM are Gauss integration and a node point scheme used by Young (1981). His implementation differs from common methods in that it uses Lobatto instead of Gauss integration. The net effect is that, while retaining the same order of integration accuracy (at least for linear and quadratic elements), there are considerably fewer nonzero terms in the resulting matrix equations. Figure 2 shows a comparison of the nodal connections for Lobatto and Gauss integration methods. It should be noted that these results hold on an orthogonal grid only. If a nonorthogonal grid were introduced, then additional nonzero terms would appear in the Lobatto quadrature method. Note also that the linear elements yield the standard 5- or 7-point difference scheme. The reader is referred to Young's paper for more details.

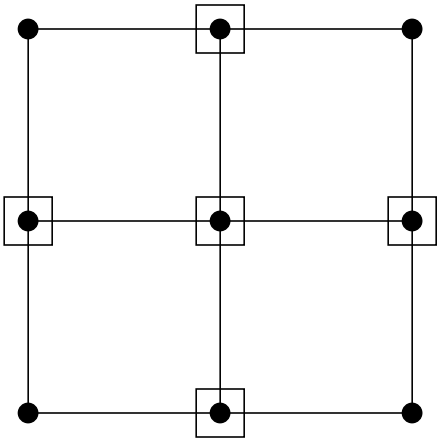

**Figure 2. Comparison of nodal connections for conventional (•) and Lobatto (□) integrations for an orthogonal grid.**

In addition to the Finite Element integration techniques described above, the code has provisions for Finite Volume calculation of the internode flow terms described by Equations (28) - (35). In the Finite Volume approach, the geometric terms are calculated as area projections and distances between nodes. The geometric part of Equations (28), (29), and (30) are given by the area between the nodes divided by the distance. The area is partitioned according to the perpendicular bisectors of the midpoints of the sides of the elements. This is shown in Fig. 3 for triangles in two dimensions. An analogous approach is used in three dimensions for tetrahedrals. Quadrilaterals in two dimensions and hexahedrals in three dimensions are first decomposed into triangles and tetrahedrals, respectively, and the geometry coefficients formed as described above. For more details the reader is referred to Fung, et al. (1994).

It is important to note here that with upwinding, the geometric factors that govern internode flow, regardless of whether calculated from a Finite Element or Finite Volume approach, must not change in sign. This requires a Delaunay grid plus the constraint that any elements at interfaces or exterior boundaries have interior angles less than $\pi/2$ radians. The reader is again referred to Fung, et al. (1994) for more details.

The development of the numerical approximation of the transport equation is similar to that for the flow equations. Following the discussion above, the species concentration, $C$, and the species accumulation term, $A_c$, are interpolated in each element: $C = [N]^T\{C\}$, $A_c = [N]^T\{A_c\}$ .

Using these approximations and a Galerkin approach, the following equation is obtained

$$[T_c(C)]\{P\} + [D_c]\{C\} + [\hat{C}]\left\{\frac{\partial A_c}{\partial t}\right\} + \{q_c\} + g\{G_c\} = \{F_c\} \qquad (36)$$

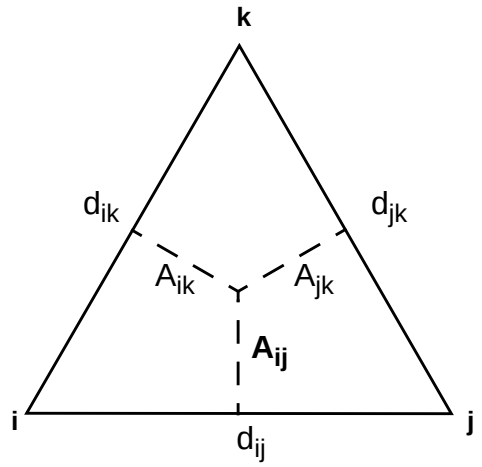


**Figure 3. Area projections and internode distances used in Finite Volume calculations on a Delaunay grid.**

where

$$T_{cij} = \int_{\Omega} \bar{\nabla} N_i \cdot D_m C_{\boldsymbol{ij}}^{UP} \bar{\nabla} N_j \, dV \,, \tag{37}$$

$$D_{cij} = \int_{\Omega} \bar{\nabla} N_i \cdot D_c \bar{\nabla} N_j \, dV \,, \tag{38}$$

$$G_{cij} = \int_{\Omega} \frac{\partial N_i}{\partial z} \cdot D_m C^{UP} \bar{\nabla} N_j \, dV \,, \tag{39}$$

and $D_m C^{UP}$ is an upstream weighted concentration transmissibility. This approach is similar to the finite difference method for solving the transport equations.

**Boundary Conditions**: Two types of fluid (mass) sources and sinks are implemented: a specified-flow-rate source/sink and a specified-pressure condition at a source/sink. No-flow or impermeable boundary conditions are automatically satisfied by the finite element mesh. The constant pressure boundary condition is implemented using a pressure dependent flow term

$$q_{m,i} = I_{m,i}(P_{flow,i} - P_i) \tag{40}$$

where $P_i$ is the pressure at the source node $i$, $P_{flow,i}$ is the specified flowing pressure, $I_{m,i}$ is the impedance, and $q_{m,i}$ is the mass flow rate. By specifying a large $I$ the pressure can be forced to be equal to $P_{flow}$. The energy (temperature) specified at a source/sink or flowing pressure node refers only to the incoming fluid value, if fluid flows out, stability dictates that the energy of the in-place fluid be used in calculations.

In addition to the mass flow source/sink, heat flow sources can also be provided. A specified heat flow can be input or a specified temperature obtained

$$q_{e,i} = I_{e,i}(T_{flow,i} - T_i) \tag{41}$$

where $T_i$ is the temperature at the source node $i$, $T_{flow,i}$ is the specified flowing temperature, $I_{e,i}$ is the impedance to heat flow (thermal resistance), and $q_{e,i}$ is the heat flow. This heat flow is superimposed on any existing heat flow from other boundary conditions or source terms. Specified saturations, relative humidities, air mass fractions as well as specified air flows are allowed. These use source/sinks to achieve the desired variable values in a way analogous to that described for pressure boundary conditions.

In FEHM there is also a provision for creating large volume reservoirs which effectively hold variables at their initial values. The nodes are labeled on input and the volumes replaced after the calculation of the geometric coefficients with a reservoir volume of $10^{13}$ $m^3$.

**Solution Method**: The application of the discretization methods to the governing partial differential equations yields a system of nonlinear algebraic equations. To solve these equations, the Newton-Raphson iterative procedure is used. This is an iterative procedure that makes use of the derivative information to obtain an updated solution from an initial guess. Let the set equations to be solved be given by

$$\{F\}(\{x\}) = \{0\} \tag{42}$$

where $\{x\}$ is the vector of unknown values of the variables that satisfy the above equation. The procedure is started by making an initial guess at the solution, say $\{x\}^0$. This is usually taken as the solution from the previous time step. Denoting the value of $\{x\}$ at the $kth$ iteration by $\{x\}^k$, the updating procedure is given by

$$\{x\}^{k+1} = \{x\}^k - \{F\}^k \left( \frac{\partial \{F\}}{\partial \{x\}^k} \right)^{-1} . \tag{43}$$

At each step, the residuals $\{F\}^k = \{F\}(\{x\}^k)$ are compared with a prescribed error tolerance. The prescribed error tolerance, $\varepsilon$, is an input parameter and an $l^2$ norm is used:

$$\|F\|_k = \left( \sum_i F_i^2 \right)_k^{1/2} . \tag{44}$$

Convergence is achieved when

$$\|F\|_k \leq \varepsilon \|F\|_o . \tag{45}$$

$\varepsilon$ is usually in the range $10^{-4}$ - $10^{-7}$. Semiautomatic timestep control is designed based on the convergence of the Newton iterations. If the code is unable to find a solution $\{x\}^k$ such that the residuals become less than the tolerance within a given number of iterations, the time step is reduced and the procedure repeated. On the other hand, if convergence is rapid, the timestep is increased by multiplying with a user supplied factor, thus allowing for large timesteps when possible.

The linear equation set to be solved at each Newton-Raphson iteration of Equation (43) is

$$\left(\frac{\partial\{F\}}{\partial\{x\}^k}\right)\{\Delta x\}^{k+1} = -\{F\}^k \tag{46}$$

where $\left(\frac{\partial\{F\}}{\partial\{x\}^k}\right)$ is the Jacobian matrix, $\{\Delta x\}^{k+1}$ is the change in the solution vector $\{\Delta x^{k+1} = x^{k+1} - x^k\}$, and $\{F\}^k$ is the residual. It is solved with a reuse component, GZSOLVE (see Zyvoloski and Robinson, 1995), that provides a robust solution method for sparse systems of equations. Further details of the solution procedure can be found in the GZSOLVE MMS.

**Reduced Degree of Freedom Algorithms:** In the coupled physical processes that describe flow in porous media, often one process is dominant. In heat and fluid flow, for example, the pressure changes more rapidly than the temperature. This fact may be used to simplify the linear equations solved at each step of a Newton-Raphson iteration and was recognized by Zyvoloski, et al. (1979). Solving the pure water heat and mass flow leads to the following set of linear equations at each Newton-Raphson iteration:

$$\begin{bmatrix} A_{mP} & A_{mT} \\ A_{eP} & A_{eT} \end{bmatrix} \begin{Bmatrix} \Delta P \\ \Delta T \end{Bmatrix} = -\begin{Bmatrix} F_m \\ F_e \end{Bmatrix} \tag{47}$$

The subscripts $m$ and $e$ refer to the mass and energy balance equations respectively. The subscripts $P$ and $T$ refer to derivatives with respect to pressure and temperature respectively. The superscripts indicating iteration number have been dropped for convenience. From Equations (9) and (10) it can be seen that the primary contribution of temperature is to affect the thermal conduction terms and the density and viscosities. Pressure, however, affects the density and is directly involved in the Darcy velocities. In other words, the pressure more directly affects the global transport of heat and mass. Guided by this reasoning, a computationally efficient scheme is obtained by neglecting the off-diagonal derivatives with

respect to temperature. With this modification the temperature change may be solved for using

$$\{\Delta T\} = [A_{eT}]^{-1}\{-\{F_e\} - [A_{eP}]\{\Delta P\}\} \tag{48}$$

This may in turn be substituted in the mass balance portion of Equation (47) giving

$$[[A_{mP}] - [A_{mT}][A_{eT}]^{-1}[A_{eP}]]\{\Delta P\} = -\{F_m\} + [A_{mT}][A_{eT}]^{-1}\{F_e\} \ . \tag{49}$$

The indicated matrix inversions and multiplications are performed with diagonal matrices and the resulting matrix for the calculation of the pressure correction is a banded matrix of exactly the same structure as $[A_{mP}]$. It was found that additional efficiency could be achieved by taking several passes of SOR iterations after the system in Equations (48) and (49) were solved (Bullivant and Zyvoloski,1990).

The same process can be used to reduce the air/water/heat coupled system to a one or two degree of freedom problem. Here the coupled 3n by 3n system may be written as

$$\begin{bmatrix} A_{mP} & A_{mT} & A_{ma} \\ A_{eP} & A_{eT} & A_{ea} \\ A_{aP} & A_{aT} & A_{aa} \end{bmatrix} \begin{Bmatrix} \Delta P \\ \Delta T \\ \Delta a \end{Bmatrix} = -\begin{Bmatrix} F_m \\ F_e \\ F_a \end{Bmatrix} \tag{50}$$

Here the subscript $a$ refers to the conservation of air mass and derivatives with respect to the air variable. The air variable is eliminated in favor of the pressure and temperature using

$$\{\Delta a\} = [A_{aa}]^{-1}\{-\{F_a\} - [A_{aP}]\{\Delta P\} - [A_{eT}]\{\Delta T\}\} \ . \tag{51}$$

Substituting this in the mass and energy correction equations:

$$\begin{bmatrix} [[A_{mP}] - [A_{ma}][A_{aa}]^{-1}[A_{aP}]] & [[A_{mT}] - [A_{ma}][A_{aa}]^{-1}[A_{aT}]] \\ [[A_{eP}] - [A_{ea}][A_{aa}]^{-1}[A_{aP}]] & [[A_{eT}] - [A_{ea}][A_{aa}]^{-1}[A_{aT}]] \end{bmatrix} \begin{Bmatrix} \Delta P \\ \Delta T \end{Bmatrix} = \begin{Bmatrix} -\{F_m\} + [A_{ma}][A_{aa}]^{-1}\{F_a\} \\ -\{F_e\} + [A_{ea}][A_{aa}]^{-1}\{F_a\} \end{Bmatrix} . \tag{52}$$

During the simulation, the phase state of the system can change. This makes it necessary to rearrange Equations (51) and (52). The method remains the same. The reduced Equations (51) and (52) are useful in thermal simulations where phase changes or other factors reduce the timestep. The 3n by 3n system may further be reduced to an n by n system. This is discussed in Bullivant and Zyvoloski (1990). Bullivant and Zyvoloski also showed that the operations given above can conveniently be done during the equation normalization process.

The last reduced degree of freedom algorithm to be described reduces the isothermal air-water problem to a one variable system. The result is similar to the Richard's solution. To obtain a computationally efficient scheme, the air pressure is constrained to atmospheric pressure in the two-phase region and the liquid saturation is constrained to 1.0 in the one-phase liquid region. The method involves switching variables and associated derivatives in the solution of the linear system that produces the Newton-Raphson correction. The matrix equation that describes the Jacobian matrices for an isothermal system is given by

$$[A_{wP}]\{\Delta P\} + [A_{wS}]\{\Delta S\} = -\{F_w\} \ . \tag{53}$$

Here the subscript $w$ refers to the water conservation equation and the subscripts $P$ and $S$ refer to derivatives with respect to pressure and saturation, respectively. Though Equation (53) has the appearance of being under constrained, for every matrix position there is only one non-zero entry in the two matrices $[A_{wP}]$ and $[A_{wS}]$. This is a consequence of the variable switching just discussed. The algorithm consists of replacing terms in $[A_{wP}]$ with terms from $[A_{wS}]$ if two-phase conditions exist at a node. The resulting system is

$$[A_{wx}]\{x\} = -\{F_w\} \tag{54}$$

where $x$ represents pressure or saturation depending on the nodal phase state.

### 8.1.7 Location

The implementation sequence for the Flow and Energy Transport Equations may be seen in Fig. 1. The box 'Form Equations, Solve Jacobian System' indicates the position in the algorithm of the components of the Flow equations in the overall structure of FEHM.

### 8.1.8 Numerical Stability and Accuracy

The equations which are solved are highly nonlinear and coupled. The stability of the system has been maximized by solving the fully coupled and fully implicit formulation of the problem. Because of the nonlinearity, however, stability cannot be guaranteed. Logic has been incorporated to restart a timestep if the code realizes it is calculating in an area where the equation of state (as implemented by FEHM) is not valid

Accuracy of the simulations is also clouded by the nonlinearity issue. Formally the spatial differencing is second order accurate and the time

terms are first order accurate. There is a provision (which is usually invoked) which upwinds the transmissibility terms. This reduces the spatial accuracy to first order. It is difficult in practice to estimate the quality of a simulation from these theoretical considerations. The user is advised to run a given problem with several grid sizes and time step sizes to assess the quality of a particular solution obtained with FEHM. The accuracy of the calculations is also addressed in the FEHM verification report (Zyvoloski and Dash, 1991).

### 8.1.9 Alternatives

The primary alternative to the formulation given here is an integrated finite difference formulation. The reader is referred to Nitao (1988) and Pruess (1991) for details. The basic difference in theory is that FEHM uses a node centered approach whereas the integrated finite difference formulation uses a cell centered approach. Classical finite differences may also be used to solve the equations presented herein but lack the geometric flexibility of the methods mentioned.

## 8.2 Dual Porosity and Double Porosity / Double Permeability Formulation

### 8.2.1 Purpose

Many problems are dominated by fracture flow. In these cases the fracture permeability controls the pressure communication in the reservoir even though local storage around the fracture may be dominated by the porous rock which communicates only with the closest fractures. This phenomena requires a model in which the fractures dominate the global pressure response of the reservoir. The fractures are needed merely as storage. Moench (1984) has studied several wells in the saturated zone beneath Yucca Mountain and found that results could be understood if dual porosity methods were used. The numerical model in which the matrix material is constrained to communicate only in the neighboring fractures is known as the Dual Porosity method.

In a partially saturated porous medium, flow is often dominated by capillary suction. In a medium comprised of fractures and matrix, the matrix material has the highest capillary suction and under relatively static conditions the moisture resides in the matrix material. Infiltration events, such as severe rainfall, can saturate the porous medium allowing rapid flow in the fractures. To capture this flow phenomena, a system of equations allowing communication between the fractures and matrix blocks in the reservoir in addition to the flow within the fractures and matrix blocks is necessary. This method is known as the Double Porosity / Double Permeability method.

The decision about which fracture model to use is often affected by the transient nature of the simulation. It is possible to obtain nearly the same results for a double permeability simulation using a less expensive equivalent continuum approach for a steady state solution but different results would be obtained for a transient solution.

For transport, the alternative fracture formulations are even more important. Here the simulations are almost always transient. The matrix and fractures are in approximate pressure equilibrium and there is little flow from matrix to fracture. The tracer in this scenario is constrained to

stay in the fracture if it started there. This often produces erroneous results that can be improved if diffusion from matrix to fracture is included. The fracture formulations in FEHM account for matrix to fracture diffusion.

### 8.2.2 Assumptions and Limitations

In the Dual Porosity method, the computational volume consists of a fracture which communicates with fractures in other computational cells, and matrix material which only communicates with the fracture in its own computational cell. This behavior of the matrix material is both a physical limitation and a computational tool. The physical limitation results from the model's inability to allow the matrix materials in different cells to communicate directly. This yields only minor errors in saturated zone calculations, but could pose larger errors in the unsaturated zone where capillary pressures would force significant flow to occur in the matrix material. The computational advantages will be addressed in Section 8.2.3.

The Double Porosity / Double Permeability method differs from the Dual Porosity method in that the matrix can communicate with other matrix nodes. This produces a more realistic simulation but is computationally more expensive.

### 8.2.3 Derivation

Figure 4 depicts the double porosity / double permeability and dual porosity concepts. Two parameters characterize a double porosity / double permeability reservoir. The first is the volume fraction, $V_f$, of the fractures in the computational cell. For the single matrix node system shown in Fig. 4 this fraction is $a/b$. The second parameter is related to the fracture's ability to communicate with the local matrix material. In the literature this parameter takes a variety of forms. The simplest is a length scale, $L_f$. This quantifies the average distance the matrix material is from the

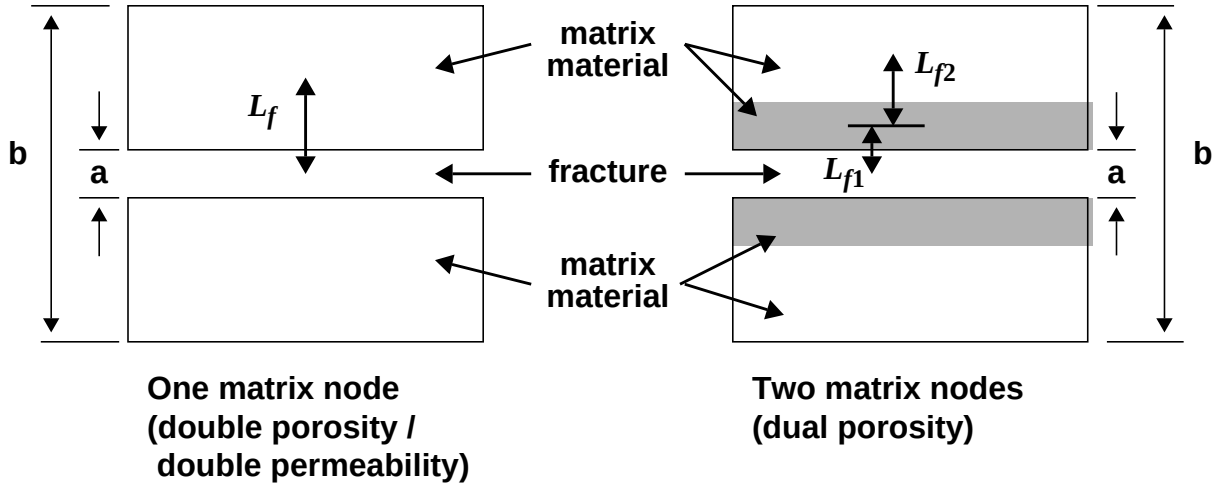


**Figure 4. Computational volume elements showing dual porosity and double porosity / double permeability parameters.**

fracture. With just one node in the matrix material the transient behavior in the matrix material cannot be modeled. To improve this situation, two nodes are used in FEHM to represent the matrix material for a dual porosity reservoir. Conceptually, this is the same formulation as just described with the addition of a second fracture volume (it is assumed the length scale of each matrix volume is proportional to the volume fraction). This is the two matrix node system shown in Fig. 4. More matrix nodes could be added, but data is rarely good enough to justify the use of even two matrix nodes. The simple slab model depicted in Fig. 4 is just one of several different geometric arrangements. Moench (1984) and Warren and Root (1963) list other reservoir types. All of them are similar in the assumption of a local one dimensional connection of the matrix to the fracture.

A volume fraction and length scale are used to characterize the system. Equations (9), (10), (20), and (76) are formulated for both the fracture and matrix computational grids. One dimensional versions are created to locally couple the two sets of equations. The length scales are used to modify spatial difference terms and the volume fractions are used to modify the accumulation terms.

The volume fractions for the double porosity / double permeability formulation satisfy the following relationship

$$V_f + V_{f1} = 1 \tag{55}$$

where $V_f$ is the volume fraction of fractures and $V_{f1}$ is the fraction of the matrix volume. The length scales are partitioned for the fracture and matrix volumes using

$$\begin{aligned} L_f &= L_{f0} V_f \\ L_{f1} &= L_{f0} V_{f1} \end{aligned} \tag{56}$$

where $L_f$ is the length scale for the fracture volume, $L_{f1}$ is the length scale of the matrix volume, and $L_{f0}$ is a characteristic length scale.

The volume fractions for the dual porosity formulation satisfy the following relationship

$$V_f + V_{f1} + V_{f2} = 1 \tag{57}$$

where $V_f$ is the volume fraction of fractures, $V_{f1}$ is the fraction of the first matrix volume, and $V_{f2}$ is the fraction of the second matrix volume. Recall that two nodes are used to model the porous rock (matrix) and the matrix material communicates only with the local fractures. The length scales are given by

$$\begin{aligned} L_f &= L_{f0} V_f \\ L_{f1} &= L_{f0} V_{f1} \\ L_{f2} &= L_{f0} V_{f2} \end{aligned} \tag{58}$$

where $L_f$ is the length scale for the fracture volume, $L_{f1}$ is the length scale of the first matrix volume, $L_{f2}$ is the length scale of the second matrix volume, and $L_{f0}$ is a characteristic length scale.

### 8.2.4 Application

The fracture models are extremely useful in investigating flow and transport in the geologic repository because of the importance of fracture flow and transport. Large differences are expected between transport calculations from lumped (matrix and fracture) properties models and models that include fracture flow and transport. FEHM through a realistic description of fractures, allows the use of more realistic radionuclide dose calculations in the performance assessment calculations.

### 8.2.5 Numerical Method Type

Only algebraic manipulations are used in the derivations described in Section 8.2.6.

### 8.2.6 Derivation of Numerical Model

#### 8.2.6.1 Dual porosity

Computationally, the volume fractions and length scales are used to create one dimensional versions of Equations (9), (10), (20), and (76). The length scale is used to modify spatial difference terms and the volume factors are used to modify the accumulation terms [the $\hat{C}$ matrix in Equations (25) and (26)].

The geometric factor representing the spatial differencing of the one dimensional equation for flow between the fracture and the first matrix node [analogous to the geometric part of Equations (28) and (29)] is given by

$$T_{ff1} = \frac{V_T}{L_{f1}(L_f + L_{f1})} \tag{59}$$

where $V_T$ is the total volume of the computational cell.

The analogous term for the flow from the first matrix volume to the second matrix volume is given by

$$T_{f1f2} = \frac{V_T}{L_{f2}(L_{f1} + L_{f2})} \tag{60}$$

Using these geometric factors Equations (25), (26), and (27) are modified with the addition of the following flux terms

$$T_{f1f2}\left(\frac{k\rho_v}{\mu_v}(P_{m,v} - P_{f,v}) + \frac{k\rho_l}{\mu_l}(P_{m,l} - P_{f,l})\right), \tag{61}$$

$$T_{f1f2}\left(\frac{k\rho_v h_v}{\mu_v}(P_{m,v}-P_{f,v})+\frac{k\rho_l h_l}{\mu_l}(P_{m,l}-P_{f,l})\right), \tag{62}$$

and

$$T_{f1f2}\left(\frac{k\rho_v h_v \eta_v}{\mu_v}(P_{m,v}-P_{f,v})+\frac{k\rho_l h_l \eta_l}{\mu_l}(P_{m,l}-P_{f,l})\right) \tag{63}$$

where $m$ refers to the matrix and $f$ to the fracture. The equation for the matrix consists of these transfer terms plus the accumulation terms analogous to those for the fracture and shown in Equations (2), (5), (19), and (24). It should also be noted that the gravity terms are not shown in the transfer terms above for simplicity but are represented in an analogous way.

The one dimensional nature of the equations provides a computationally efficient method to solve the algebraic equations arising from the dual porosity simulation. Equation (64) shows the matrix equation arising from a dual porosity simulation.

$$\begin{bmatrix} A_{00} & A_{01} & A_{02} \\ A_{10} & A_{11} & A_{12} \\ A_{20} & A_{21} & A_{22} \end{bmatrix} \begin{Bmatrix} x_0 \\ x_1 \\ x_2 \end{Bmatrix} = -\begin{Bmatrix} b_0 \\ b_1 \\ b_2 \end{Bmatrix} \tag{64}$$

Here the subscript 0 refers to the fracture, 1 refers to the first matrix volume, and 2 refers to the second matrix volume. The $x$ represents the unknown variable or variable pair. The one dimensional character of the matrix diffusion means that the second matrix node can only depend on the first matrix node. Therefore, the submatrix $[A_{20}]$ is empty. The fact that matrix nodes cannot communicate with matrix nodes in other computational cells means that the submatrices $[A_{21}]$ and $[A_{22}]$ are diagonal, therefore

$$\{x_2\} = [A_{22}]^{-1}[-\{b_2\}-[A_{21}]\{x_1\}] \tag{65}$$

where the inversion is trivial because $[A_{22}]$ is diagonal. Substituting this expression into the equation for the first matrix node gives

$$[A_{10}]\{x_0\}+[A_{11}]\{x_1\}+ [A_{12}][A_{22}]^{-1}[-\{b_2\}-[A_{21}]\{x_1\}] = -\{b_1\} \tag{66}$$

Rearranging,

$$[A_{10}]\{x_0\} + [[A_{11}] - [A_{12}][A_{22}]^{-1}[A_{21}]]\{x_1\} =$$
$$-\{b_1\} + [A_{12}][A_{22}]^{-1}\{b_2\}$$

or

$$\{x_1\} = [\tilde{A}_{11}]^{-1}[\{\tilde{b}_1\} - [A_{10}]\{x_0\}] \quad (67)$$

where

$$[\tilde{A}_{11}] = [A_{11}] - [A_{12}][A_{22}]^{-1}[A_{21}] \quad (68)$$

and

$$\{\tilde{b}_1\} = -\{b_1\} + [A_{12}][A_{22}]^{-1}\{b_2\} \ . \quad (69)$$

The inversion and multiplications are trivial because of the diagonal nature of the matrices involved. Equation (67) may next be substituted into the equation for the fracture variables. Noting that $[A_{02}]$ is empty (the fracture can only communicate with the first matrix volume) gives

$$[A_{00}]\{x_0\} + [A_{01}][\tilde{A}_{11}]^{-1}[\{\tilde{b}_1\} - [A_{10}]\{x_0\}] = -\{b_0\} \ . \quad (70)$$

Rearranging terms results in

$$[[A_{00}] - [A_{01}][\tilde{A}_{11}]^{-1}[A_{10}]]\{x_0\} = -\{b_0\} + [A_{01}][\tilde{A}_{11}]^{-1}\{\tilde{b}_1\} \quad (71)$$

Equation (71) consists of an augmented fracture matrix of the same form as the original fracture matrix $[A_{00}]$. The operations carried out only add a few percent to the solution time required to solve a single porosity system. After the solution of Equation (71) is obtained with the methods described in the GZSOLVE MMS, the solution in the fracture volume can be obtained by using Equations (65) and (67).

#### 8.2.6.2 Double Porosity / Double Permeability

The Double Porosity / Double Permeability method is analogous to the Dual Porosity method described above with the exception that there is only one matrix node represented in the Double Porosity / Double Permeability method. The matrix node, however, can communicate globally to other matrix nodes. This leads to a system of equations of the form

$$\begin{bmatrix} A_{00} & A_{01} \\ A_{10} & A_{11} \end{bmatrix} \begin{Bmatrix} x_0 \\ x_1 \end{Bmatrix} = - \begin{Bmatrix} b_0 \\ b_1 \end{Bmatrix} \quad (72)$$

In this system of linear equations, the submatrices $A_{00}$ and $A_{11}$ are sparse and $A_{01}$ and $A_{10}$ are diagonal. Currently this system of linear equations is solved directly, but research to improve the efficiency of solution is ongoing.

### 8.2.7 Location

When enabled the fracture models are called during the equation generation and solution phases of the simulation. This is the same place as shown for the Flow and Transport models in Fig. 1.

### 8.2.8 Numerical Stability and Accuracy

The same considerations that were discussed in Section 8.1.8 for the Flow and Transport models are valid here.

### 8.2.9 Alternatives

Other approaches to modeling fractures include the equivalent continuum approach, in which the fracture and matrix properties are averaged, and the discrete fracture approach, in which the fractures are modeled as individual computational cells. Both of these methods are included in the model described in Section 8.1, “Flow and Energy Transport”.

There has also been some effort to use a combination of numerical and analytic techniques. In this approach the matrix flow is represented with a one dimensional analytic expression. Because of the nonlinear nature of the solution, this approach has not been pursued.

## 8.3 Solute Transport - Reactive Transport and Particle Tracking Models

### 8.3.1 Purpose

The purpose of the reactive transport and particle tracking models are to simulate the movement of tracer solutes traveling in either the liquid or gas phases. A variety of reactive transport capabilities are present in the models. To perform a reactive transport simulation, an initial description of each solute concentration in each phase, transport properties of the fluid and medium, and a specification of the adsorption model and parameters and any reaction models are required. The output consists of the final concentration of each solute in each phase.

### 8.3.2 Assumptions and Limitations

Solutes are assumed to be present in trace quantities, such that their presence does not impact the fluid properties or the computed flow fields. A related assumption is that chemical reactions do not enter into the energy balance through endothermic or exothermic reaction terms. If reactions take place between the fluid and solid phases (dissolution and precipitation), the transfer of mass is assumed to have no impact on the hydrologic properties of the medium.

Many other specific assumptions are built into the solute transport models related to the nature of the transport and chemical reaction behavior. These assumptions are treated in Section 8.3.3.

### 8.3.3 Derivation

#### 8.3.3.1 Reactive Transport Model

The solute transport equations in the reactive transport model are not directly coupled to the heat and mass transfer system, but use the flow rates and temperatures obtained by the heat and mass transfer solution. The mass flux, $\overline{f_c}$, source (or sink) strength, $q_c$, and accumulation term, $A_c$, are defined as follows for a solute:

$$\overline{f_c} = C_v \rho_v \overline{v_v} + C_l \rho_l \overline{v_l} \ , \tag{73}$$

$$q_c = C_v q_v + C_l q_l \ , \tag{74}$$

$$A_c = \phi (C_v S_v \rho_v + C_l S_l \rho_l) \ . \tag{75}$$

The transport equation for a solute is given by

$$-\overline{\nabla} \cdot (C_v D_{mv} \overline{\nabla} P_v) - \overline{\nabla} \cdot (C_l D_{ml} \overline{\nabla} P_l) - \overline{\nabla} \cdot (D_{cv} \overline{\nabla} C_v) - \overline{\nabla} \cdot (D_{cl} \overline{\nabla} C_l) +$$
$$q_c + \frac{\partial}{\partial z} g (C_v D_{mv} \rho_v + C_l D_{ml} \rho_l) + \rho_r \frac{\partial C_R}{\partial t} + \frac{\partial A_c}{\partial t} = 0 \ . \tag{76}$$

Here $C$ is the concentration of the solute. The term $\overline{\nabla} \cdot (D_c \overline{\nabla} C)$ is the dispersion term and $\rho_r \frac{\partial C_r}{\partial t}$ is an equilibrium sorption term (see section below for the formulation for sorbing solutes). $C_r$ represents the adsorption of the solute onto the porous media. In addition, the term $q_c$ includes the source or sink due to chemical reaction. The chemical reaction terms are discussed in more detail below in the section titled “Chemical Reaction Module.”

Equation (76) is a general equation for a solute present in either the liquid or gas phases, or one that partitions between the liquid and gas. The model is capable of simulating any of these possibilities, as well as a solid species, for which only the accumulation and chemical reaction terms are present. Several solutes can be simulated simultaneously, and can interact with one another through the chemical reaction model. The transport terms can be set as a function of position, and there is no requirement that they be the same for all solutes present in a phase.

The next four subsections elaborate on various transport, sorption, and reaction features of the reactive transport model.

**Dispersion Coefficients.** The model uses a standard formulation for the dispersion coefficient, expressed as follows for the x-direction

$$D_{cl,\,x} = D_{AB} + \alpha_{dl,\,x} v_{l,\,x} \ . \tag{77}$$

The Darcy velocity is computed from the solution of the fluid flow equation. The dispersivity $\alpha_d$ and the molecular diffusion coefficient $D_{AB}$ are properties of the medium, the fluid (liquid in the above equation) and the solute. Similar expressions are written for the y- and z-directions.

**Adsorbing Solutes**. The general equilibrium model for adsorption of species onto the reservoir rock is given by Polzer, et al. (1992):

$$C_r = \frac{\alpha_1 C_l^{\beta}}{1 + \alpha_2 C_l^{\beta}} \ . \tag{78}$$

The parameters $\alpha_1$, $\alpha_2$, and $\beta$ are given in Table II along with the commonly used sorption isotherm models that can be derived from the equation. The parameters $K_d$, $\Lambda$, $C_{max}$, $r_b$, and $r$ are the corresponding parameters associated with the sorption models as they are more commonly formulated. For example, when the linear, equilibrium sorption model is selected, the $\alpha_1$ parameter is the widely used $K_d$ parameter cited in sorption studies.

**Table II. Sorption Isotherm Models**‡

| Model | Expression | $\alpha_1$ | $\alpha_2$ | $\beta$ |
|---|---|---|---|---|
| *Linear* | $C_r = K_d C_l$ | $K_d$ | 0 | 1 |
| *Freundlich* | $C_r = \Lambda C_l^{\beta}$ | $\Lambda$ | 0 | $0 < \beta < 1$ |
| *Modified Freundlich* | $\frac{C_r}{C_{r,\,max} - C_r} = \Lambda C_l^{\beta}$ | $\Lambda C_{r,max}$ | $\Lambda$ | $0 < \beta < 1$ |
| *Langmuir* | $C_r = \frac{r_b C_l}{1 + r C_l}$ | $r_b$ | $r$ | 1 |

‡ from Robinson (1993)

To solve the solute mass balance equation with equilibrium sorption, $C_R$ in Equation (76) is computed using Equation (78) to determine the mass of solute on the rock for a given fluid-

phase concentration. Thus, $C_R$ is not actually present as a separate unknown in the mass balance.

**Multiple, Interacting Solutes**. Thus far, only the specification of an individual solute has been discussed. In the reactive transport model, chemical reactions involving one or more components can be specified. FEHM uses aqueous, immobile and vapor components as the primary dependent variables (PDVs) in the reactive transport equations. A set of chemical components is defined as the minimum number of species that uniquely describe the chemical system (Mangold and Tsang, 1991). In FEHM, the secondary dependent variables (SDVs) are uncomplexed aqueous component concentrations and aqueous complex concentrations. We assume that all aqueous phase speciation reactions are at equilibrium (known as the local equilibrium assumption), resulting in the following relationship between PDVs and SDVs:

$$C_j = c_j + \sum_{i=1}^{N_x} a_{ij} x_i \qquad j = 1, \ldots, N_c \qquad (79)$$

where $C_j$ is the total aqueous concentration of component $j$, $c_j$ is the uncomplexed concentration of component $j$, $x_i$ is the concentration of complex $i$, $a_{ij}$ is the stoichiometric coefficient representing the number of moles of component j in complex $i$, $N_c$ is the number of aqueous components and $N_x$ is the number of aqueous complexes (Yeh and Tripathi, 1989).

Applying the local equilibrium assumption to aqueous phase speciation reactions greatly reduces the number of PDVs in the transport equations and is generally accepted to be a valid assumption (e.g. Steefel and Lasaga, 1994). Given the total aqueous concentration of each aqueous component, the SDVs can be calculated using a set of nonlinear algebraic equations derived from chemical equilibrium theory (e.g. Lichtner, 1996). In order to obtain the total aqueous concentrations, the reactive transport equations for aqueous, immobile, and vapor components must be solved. There are no SDVs for either vapor and immobile components, since the model as currently formulated treats only aqueous speciation. Reactions involving vapor and immobile components are treated with a kinetic formulation, with kinetic reactions represented as reaction source-sink terms in the reactive transport equations.

*Governing Equations for the PDVs:* For convenience, we rewrite equation (76) into the following form for a total aqueous component:

$$\frac{\partial A_j}{\partial t} = \nabla\bullet(\phi S_l D_j \nabla \rho_l C_j) - \nabla\bullet f_c + R_j \qquad j = 1, \ldots, N_c \quad (80)$$

where $A_j = \phi C_j S_l \rho_l$ is the solute mass storage per unit total volume for aqueous component liquid concentration $C_j$ (units of concentration are moles/kg fluid); $f_c = \rho_l C_j u_l$ is the advective mass flux of solute; $D$ is the hydrodynamic dispersion tensor; $S_l$ is the saturation; $u_l$ is the Darcy velocity vector; $\phi$ is the porosity; $S_l$ is the liquid saturation; and $R_j$ is the kinetic reaction source-sink term. To simplify the notation for the remainder of the reactive transport section, we define the advection-dispersion operator:

$$L_l(C) = \nabla\bullet f_c - \nabla\bullet(\phi S_l D_j \nabla \rho_l C_j) \quad (81)$$

Equation (81), the reactive advection dispersion equation, can then be rewritten as:

$$\frac{\partial A_j}{\partial t} + L_l(C_j) = R_j \qquad j = 1, \ldots, N_c \quad (82)$$

The reaction transport equation for a vapor component takes on a similar form to Equation (83) and is given by

$$\frac{\partial A_k}{\partial t} + L_v(G_k) = R_k \qquad k = 1, \ldots, N_v \quad (83)$$

where $A_k$ is the solute mass per total volume of component *k*, $G_k$ is the vapor concentration of component *k*, $u_v$ is the vapor Darcy velocity vector and $N_v$ is the number of vapor components. The hydrodynamic dispersion tensor is assumed to reduce to longitudinal and transverse components (e.g. Lichtner, 1996).

Immobile components are not transported and are therefore treated using a simple mass balance given by

$$\frac{\partial M_m}{\partial t} = R_m \qquad m = 1, \ldots, N_{im} \quad (84)$$

where $M_m$ is the immobile concentration (mass solute per unit mass rock matrix) of component m and $N_{im}$ is the number of immobile components.

The reaction rate terms in Equations (82), (83), and (84) originate from the kinetic reactions in the system and may be nonlinear functions of the concentrations of the total aqueous components, uncomplexed aqueous components, aqueous complexes, immobile components and vapor components. FEHM is capable of modeling the following kinetic processes: linear adsorption, nonlinear Langmuir adsorption, ion/surface exchange, precipitation-dissolution and liquid-vapor interchange of solute. Equations (82), (83), and (84) result in a system of $(N_c + N_{im} + N_v)N_n$ nonlinear coupled partial differential equations (PDEs) where $N_n$ is the number of spatial grid points. FEHM's method for solving this system of coupled PDEs will be discussed in the solution procedure section.

*Governing Equations for the SDVs:* Given all of the aqueous component concentrations, the uncomplexed aqueous component concentrations and aqueous complex concentrations can be calculated using chemical equilibrium theory. The chemical equilibrium calculations performed by FEHM are similar to the techniques used in batch geochemical software such as EQ3/6 (Wolery, 1992). A chemical reaction describing aqueous speciation can be written in the following general form

$$\sum_{j=1}^{N_c} a_{ij}\hat{C}_j \Leftrightarrow \hat{X}_i \qquad i = 1, \ldots, N_x \qquad (85)$$

where $\hat{C}_j$ is the chemical formula for the aqueous component *j*, and $\hat{X}_i$ is the chemical formula for the aqueous complex *i*. FEHM assumes that all aqueous speciation reactions are at local equilibrium. The mass action expression for an aqueous component is given by

$$K_i = x_i \prod_{j=1}^{N_c} (\gamma_j c_j)^{-a_{ij}} \qquad (86)$$

where $K_i$ is the equilibrium formation constant for complex *i* and $\gamma_j$ is the activity coefficient for aqueous component *j*. In FEHM, we neglect ionic strength corrections. Equations (79) and (86) can be combined to express the total aqueous concentration of component j as a function of the uncomplexed component concentrations:

$$C_j = c_j + \sum_{i=1}^{N_x} a_{ij} K_i \prod_{z=1}^{N_c} c_z^{a_{iz}} \qquad j = 1, \ldots, N_c \qquad (87)$$

Equation (87) results in a set of $N_c$ nonlinear algebraic equations to be solved given all of the total aqueous concentrations.

*Kinetic Reactions:* Kinetic reactions modeled by FEHM cannot be described by a single reaction rate expression. Rate expressions are available to simulate sorption, precipitation/ dissolution, dual Monod biodegradation, and a general reversible reaction. Additional kinetic rate expressions can be included by adding subroutines that contain the reaction rate and the derivative of the reaction rate as a function of free ion, complex or total component concentrations. Note that the kinetic rate expressions do not necessarily conserve charge. In all of the reactive transport systems modeled, we do not attempt to model the complete set of chemical reactions, but attempt to model a simplified set of reactions. Since all reactions are not included, a charge balance on the entire system is not possible.

The sorption models we use in the current study contain the same parameters that are measured in laboratory and field experiments for the various applications we have investigated. For this reason, we have chosen a linear kinetic sorption, and a kinetic ion-exchange model. The retardation of contaminants due to adsorption/desorption can be modeled with a linear kinetic sorption/desorption expression. The rate of adsorption/ desorption of component j is given by:

$$R_j = -k_m \left( c_j - \frac{m_j}{K_D} \right) \qquad (88)$$

where $k_m$ is the mass transfer coefficient, and $K_D$ is the distribution coefficient. As $k_m \rightarrow \infty$, this expression reduces to the linear equilibrium isotherm.

Biodegradation is an irreversible process in which bacteria oxidize an organic substrate to produce energy and biomass. In addition to biomass, the biodegradation process requires the presence of an electron acceptor (e.g. oxygen, nitrate, etc.) and nutrients (e.g. nitrogen and phosphorous). An example of a simplified biodegradation reaction is given by the following reaction:

Substrate + Electron Acceptor + Nutrients -> cells + $CO_2$ + $H_2O$

FEHM models the rate of biodegradation of a substrate with a multiplicative Monod model, which is given by:

$$R_s = -q_m m_b \frac{[S]}{K_s + [S]} \frac{[A]}{K_A + [A]} \tag{89}$$

where $[S]$ is the aqueous concentration of substrate (a.k.a the electron donor), $[A]$ is the aqueous concentration of the electron acceptor, and $m_b$ is the concentration of the immobile biomass. The parameter $q_m$ is the maximum specific rate of substrate utilization, which represents the maximum amount of substrate that can be consumed per unit mass of bacteria per unit time. The parameters $K_S$ and $K_A$ are the Monod half-maximum-rate concentrations for the electron donor and electron acceptor, respectively. The rate of microbial growth is given by the synthesis rate (which is proportional to the rate of substrate degradation) minus a first-order decay rate.

$$R_{cells} = -YR_s - b(m_b - m_{b,\,init}) \tag{90}$$

where $Y$ is the microbial yield coefficient and $b$ is the first-order microbial decay coefficient. In the above equation, the assumption is made that the background conditions are sufficient to sustain a microbial population of a given size; therefore, the biomass concentration is not allowed to fall below its initial background concentration ($m_{b,init}$).

A general reaction describing the precipitation/dissolution of a mineral p can be written in the following form:

$$m_p \Leftrightarrow \mu_{p1} c_1 + \mu_{p1} c_2 + \ldots + \mu_{p1} c_{N_c} \tag{91}$$

where $c_j$ are the aqueous concentrations, $\mu_{pj}$ are stoichiometric coefficients. The equilibrium constant for this reaction is known as the solubility product. Since the activity of a pure solid is equal to one, the reaction quotient $Q_p$ is defined as follows:

$$Q_p = \prod_{j=1}^{N_c} c_j^{\mu_{pj}} \tag{92}$$

At equilibrium, $Q_p$ is equal to the solubility product. The surface-controlled rate of precipitation/dissolution of a mineral is given by:

$$\frac{dC_j}{dt} = \frac{A_s}{V} \mu_j k_+ \left(1 - \frac{Q_p}{K_{sp}}\right) \tag{93}$$

where $C_j$ is the concentration of component *j* in solution, $A_s$ is reactive surface area of the mineral, $k_+$ is the rate constant, and $K_{sp}$ is the solubility product. With this equation, a mineral will precipitate when it is supersaturated and dissolve when it is undersaturated.

**Solute Sources and Sinks.** Solute sources or sinks are handled in a manner analogous to the fluid flow sources and sinks. If there is fluid flow out of the model domain (a fluid sink), the in-place solute concentration is used in the solute mass balance. For fluid entering the system, the solute concentration of the incoming fluid can be specified. Alternatively, the concentration at a node or nodes can be held at a fixed concentration. This boundary condition can be either a source or sink for solute, depending on the gradient in concentration at locations adjacent to the node at which the boundary condition is applied.

Occasionally, it is desirable to simulate a situation in which water exiting the system leaves the solute behind rather than removing it. For example, if water vapor is removed from the model due to evaporation, a liquid solute would not be removed, but rather would remain in the model domain and the concentration would rise. The code also has an option to implement this type of boundary condition.

#### 8.3.3.2 Particle Tracking Model

The particle tracking method developed in FEHM views the fluid flow computational domain as an interconnected network of fluid storage volumes. The description that follows is applicable for steady state flow fields; the variations in the method for treating transient flow systems are discussed later. The two steps in the particle tracking approach are: 1) determine the time a particle spends in a given cell, and 2) determine which cell the particle travels to next. These two steps are detailed below.

The residence time that a particle spends in a cell is governed by a transfer function describing the probability of the particle spending a given length of time in the cell. Thus, this particle tracking approach is called the “residence time transfer function” (RTTF) method. For a cumulative probability distribution function of particle residence times, the residence time of a particle in a cell is computed by generating a random number between 0 and 1, and determining the corresponding residence time. If a large number of particles pass through the cell, the cumulative residence time distribution (RTD) of particles in the cell will be reproduced.

From the solution of the flow field in a numerical model, the mass of fluid in the computational cell, and the mass flow rate to or from each adjacent cell is obtained. In the simplest case,

the residence time of a particle within each finite difference cell $\tau_{part}$ is given by

$$\tau_{part} = \tau_f = \frac{M_f}{\sum \dot{m}_{out}} \tag{94}$$

where $M_f$ is the fluid mass associated with the cell and the summation term in the denominator refers to the outlet mass flow rates from the cell to adjacent cells. In the absence of dispersion or other transport mechanisms, the transfer function is a Heaviside function that is unity at the fluid residence time $\tau_f$, since for this simple case all particles possess this residence time. Equilibrium, linear sorption is included by correcting the residence time by a retardation factor $R_f$, so that $\tau_{part} = R_f \tau_f$, where $R_f$ is given by

$$R_f = 1 + \frac{\rho_b K_d}{\phi S_f \rho_f} \ . \tag{95}$$

In Equation (95), $K_d$ is the equilibrium sorption coefficient, $\rho_b$ is the bulk rock density, $\phi$ is the porosity, $S_f$ is the saturation of the phase in which the particle is traveling, and $\rho_f$ is the density of the fluid. Once again, in the absence of other transport processes, the transfer function is a Heaviside function.

Before discussing more complex examples of the RTTF method, the method for determining which cell a particle travels to after completing its stay at a given cell is outlined. The assumption that is consistent with the RTTF method is that the probability of traveling to a neighboring cell is proportional to the mass flow rate to that cell. Only outflows are included in this calculation; the probability of traveling to an adjacent node is 0 if flow is from that node to the current node. By generating a uniform random number from zero to one, the decision of which node to travel to is straightforward. Thus the particle tracking algorithm is: 1) compute the residence time of a particle at a cell using the RTTF method; and 2) send the particle to an adjacent cell randomly, with the probability of traveling to a given cell proportional to the mass flow rate to that cell.

The transfer function for transport processes such as dispersion are described now. Within a computational cell, it is assumed that one-dimensional, axial dispersion is valid. The transport equation and boundary conditions for the one-dimensional, advective-dispersion equation are

$$R_f \frac{\partial C}{\partial t} = D_{eff} \frac{\partial^2 C}{\partial x^2} - v \frac{\partial C}{\partial x} , \tag{96}$$

$$C = C_{in} \qquad \text{at } x = 0 \text{ and} \tag{97}$$

$$\frac{\partial C}{\partial x} = 0, \qquad \text{for } x \to \infty . \tag{98}$$

In the equations above, $C$ is the concentration, $C_{in}$ is the injection concentration, $v$ is the superficial flow velocity, and $D_{eff}$ is the effective dispersion coefficient, given by $D_{eff} = \alpha v$, where $\alpha$ is the dispersivity of the medium. Here it is assumed that the flow dispersion component of $D_{eff}$ is large compared to the molecular diffusion coefficient $D_{AB}$. A nondimensional version of Equation (96) can be obtained using the following transformations: $\hat{C} = C/C_{in}$, $\hat{x} = x/L$, $\hat{\theta} = R_f vt/L = R_f \tau_f$, where $L$ is the distance along the flow path where the concentration is being measured. Then, Equation (96) becomes

$$\frac{\partial}{\partial \hat{\theta}} \hat{C} = Pe^{-1} \frac{\partial^2}{\partial \hat{x}^2} \hat{C} - u \frac{\partial}{\partial \hat{x}} \hat{C} \tag{99}$$

where $Pe = vL/D_{eff}$ is the Peclet number. Alternatively, $Pe = L/\alpha$. The solution to this equation and boundary conditions is given by Brigham (1974) as

$$\hat{C} = \frac{1}{2}\left[ erfc\left( \frac{\sqrt{Pe}(1-\hat{\theta})}{2\sqrt{\hat{\theta}}} \right) + e^{Pe} erfc\left( \frac{\sqrt{Pe}(1+\hat{\theta})}{2\sqrt{\hat{\theta}}} \right) \right] . \tag{100}$$

The use of this solution in the RTTF particle tracking method requires that the transport problem be advection dominated, so that during the time spent in a computational cell, solute would not tend to spread a significant distance away from that cell. Then, the approximate use of a distribution of times within the cell should be adequate. Quantitatively, the criterion for applicability is based on the grid Peclet number $Pe_g = \Delta x/\alpha$, where $\Delta x$ is the characteristic length scale of the computational cell. Note that in contrast to conventional solutions to the advective-dispersion equations, coarse spatial discretization is

helpful in satisfying this criterion, as long as the mesh spacing is small enough to provide an accurate flow solution. Highly dispersive transport invalidates the assumptions of the RTTF particle tracking technique. This is not viewed as a severe limitation of the method, since accurate solutions to the advective-dispersion equation are easily obtained by conventional finite difference or finite element techniques for this case. The niche filled by this new technique is in the solution of advection-dominated problems involving the movement of sharp concentration fronts.

For multi-dimensional flow systems, this method for simulating dispersion can be extended for the case of dispersion coefficient values aligned with the coordinate axes. For this case, the flow direction is determined by the vector drawn from the nodal position of the cell the particle traveled from to the current cell, and the dispersivity for this flow direction is given by

$$\alpha = \frac{\Delta x \alpha_x + \Delta y \alpha_y + \Delta z \alpha_z}{L} \quad . \tag{101}$$

The RTTF particle tracking technique cannot be formulated with a longitudinal and transverse dispersion coefficient model, since the flow rates between cells are defined, rather than the actual flow velocity at a position. For a dispersion model aligned to the flow direction, the particle tracking method such as that of Tompson and Gelhar (1990) or a conventional finite element or finite difference solution to the advective-dispersion equation should be used.

**Matrix Diffusion.** Matrix diffusion has been recognized as an important transport mechanism for fractured porous media (Neretnicks, 1980, Robinson, 1994). For many hydrologic flow systems, fluid flow is dominated by fractures, because of the orders of magnitude larger permeabilities in the fractures compared to the surrounding rock matrix. However, even when the fluid in the matrix is completely stagnant, solute can move into the matrix via molecular diffusion, resulting in a physical retardation of solute compared to pure fracture transport. This effect has recently been demonstrated at the laboratory scale by Reimus (1995), and at the field scale by Maloszewski and Zuber (1985).

To develop a transfer function for matrix diffusion, an idealized representation of the transport system must first be developed. Figure 5 shows the geometry of the model system used for this purpose. The geometry and flow system consists of equally spaced, parallel fractures, each of which transmits equal flow. Fluid in the rock matrix is stagnant. Transport in the fractures is governed by Equation (96) with an additional term $q_{fm}$ on the right hand side, given by

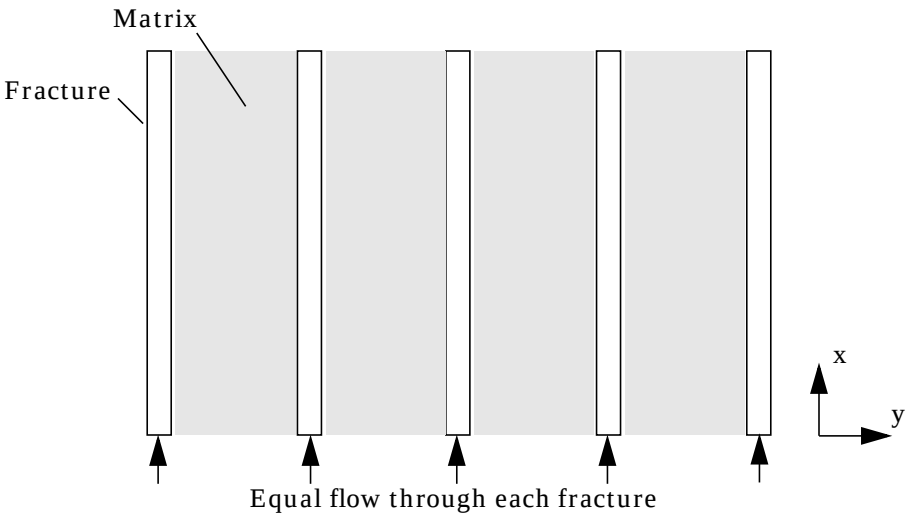


**Figure 5. Model system used to formulated the residence time transfer function for matrix diffusion**

$$q_{fm} = \frac{2\phi_{mat} D_{AB} \frac{\partial C}{\partial y}\Big|_{y = b/2}}{b_f} \tag{102}$$

where $\phi_{mat}$ is the matrix porosity and $b_f$ is the fracture aperture. Transport between the fracture and matrix is governed by the one-dimensional diffusion equation:

$$R_{f,m} \frac{\partial C}{\partial t} = D_{AB} \frac{\partial^2 C}{\partial y^2} \tag{103}$$

where $R_{f,m}$ is the retardation coefficient for the matrix. The molecular diffusion coefficient is a function of the free diffusion coefficient of the solute in water and a tortuosity factor to account for the details of diffusion through the tortuous, fluid filled pore network. In this model, $D_{AB}$ is treated as the fundamental transport parameter, recognizing that it is a property of both the solute and the medium. Solutions to this transport problem depend on the nature of the boundary condition away from the fractures. An analytical solution is given by Tang, et al. (1981) for the semi-infinite boundary condition $\frac{\partial C}{\partial y} = 0$ as $y \rightarrow \infty$. For the case of plug flow (no dispersion) in the fractures, Starr, et al. (1985) show that the solution reduces to

$$\hat{C} = erf\left[\frac{\phi_{mat}\tau_f\sqrt{R_{f,m}D_{AB}}}{b_f\sqrt{t - R_f\tau_f}}\right] . \quad (104)$$

The semi-infinite boundary condition between fractures limits the validity of either of these solutions to situations in which the characteristic diffusion distance for the transport problem is small compared to the fracture spacing. However, as long as the solute has insufficient time to diffuse to the centerline between fractures, the solutions provided by Tang, et al. (1981) or Starr, et al. (1985) are valid to represent the transfer function for the particle tracking technique.

Although in principal the Tang, et al. (1981) solution could be used for the transfer function, its complex form makes it very inconvenient for rapidly computing particle residence times. Instead, a two-step process is used in which the residence time within the fracture is first computed using the transfer function for one-dimensional dispersion in Equation (100) without sorption. Then, the plug-flow equation with matrix diffusion and sorption (Equation (104)) is used with the value of the fracture residence time just determined to set the transfer function for the matrix diffusion component of the model. To use Equation (104) as a transfer function, a subroutine was developed to determine the inverse of the error function, that is, the value of $x_d$ for a given value of $y_d$, such that $y_d = erf(x_d)$ . The numerical implementation of this method entails dividing the error function into piecewise continuous segments from which the value of $x_d$ is determined by interpolation. The use of the two-step approach is justified because of the principle of superposition, which allows the decoupling of the dispersive process in the fracture from the diffusive transport in the matrix.

**Radioactive decay.** Radioactive decay is important to many of the applications for which this model was developed, namely nuclear waste repository studies. Natural isotopes such as $^{36}$Cl and $^{14}$C also require the simulation of radioactive decay. This phenomenon can be treated by introducing the decay equation for an irreversible first order reaction:

$$\hat{C} = \exp(-k_{Rn}\tau_{age}) \quad (105)$$

where $\tau_{age}$ is the particle age since entering the system, and $k_{Rn}$ is the rate constant for radioactive decay, related to the radioactive decay half-life $\tau_{1/2}$ by $k_{Rn} = 0.693/\tau_{1/2}$.

In this model, the concept of a fraction of a particle is used to incorporate radioactive decay into the calculation. The age of a particle, or time since entering the system, is used in Equation (105) to compute the fraction of the particles remaining at the current time. When concentration values are computed from the composite behavior of a large number of particles, this method accurately accounts for radioactive decay.

**Particle Sources and Sinks.** There are two methods for introducing particles into the flow system: 1) inject the particles with the source fluid entering the model domain, or 2) release the particles at a particular node or set of nodes. The first method is used to track injected fluid as it passes through the system. The number of particles entering with the source fluid at each cell is proportional to the source flow rate at that node. The method is the particle tracking equivalent to a constant solute concentration in the source fluid. For method 2, an equal number of particles are released at each node specified, regardless of the source flow rate. In either case, the model calls for the particles to be released over a specified time interval. The code then computes a starting time for each particle.

For fluid exiting the model domain, the model treats this flow as another outlet flow from the node. The decision of whether the particle leaves the system or travels to an adjacent node is then made on a probabilistic basis, just as though the fluid sink were another connected node. When a particle leaves the system, its sojourn through the model domain is completed; this fact is recorded as part of the statistics of the simulation.

**Transient Flow Fields.** When RTTF particle tracking method is implemented for a time varying fluid flow system, the approach is somewhat more complex but still tractable. Consider a numerical simulation in which a discrete time step is taken at time $t$, and a new fluid flow field is computed. In this model, transient flows are handled by treating the new fluid flow time $t_{new}$ as an intermediate time in the particle tracking calculation that the simulation must stop at. The fate of all particles is tracked from time $t$ to time $t_{new}$ assuming that the flow field is constant over this time interval. When the simulation reaches $t_{new}$, the position of the particle is recorded, along with the fractional time remaining for the particle at the cell, and the randomly generated y-coordinate of the transfer function used for that particle in the cell. When the new fluid flow solution is established, the process continues, but the remaining residence time for a particle is the time determined from the new transfer function times the fractional time remaining in the cell.

Another transient effect that must be considered is that the sum of the outlet mass flow rates $\sum \dot{m}_{out}$ in Equation (94) does not

necessarily equal the sum of the inlet mass flow rates. When there is net fluid storage in a cell, the particle tracking algorithm uses the sum of the inlet flow rates in Equation (94), whereas Equation (94) itself is used when there is net drainage of fluid.

### 8.3.4 Applications

For transport calculations using either the reactive transport or particle tracking models, the validity of the solution depends first on the accuracy of the flow equations. In addition, the reliability of the transport parameters is also a factor in the representativeness of any transport simulation.

For the reactive transport model, the issue of numerical accuracy is extremely important to the usefulness of the results. The accuracy may be evaluated by solving the same problem using different size grids and evaluating the change in the solution. The major source of numerical errors for transport solutions is anticipated to be the numerical dispersion resulting from the upwinding of the advection term. Alternatively, the particle tracking module can be used for advection-dominated problems to provide a solution that can be compared to the reactive transport results.

The primary applications of the particle tracking model are:

- To generate transport solutions that are able to track sharp fronts in concentration without numerical dispersion, thereby allowing results from the reactive transport model to be evaluated for numerical accuracy;
- To allow fluid pathways to be mapped out visually using particles that follow the fluid;
- To provide a transport solution for a solute that diffuses into the rock matrix;
- To compile statistics on the distribution of fluid ages present at a given location.

Several limitations of the particle tracking model should be noted. The particle tracking method produces a transport solution that is free of numerical dispersion when flow is predominantly aligned with the fluid flow finite element grid. Grid orientation effects may be present when flow travels diagonally across the grid. The dispersion model extends the transport solution beyond a simple “plug flow” transport model, but the RTTF method is only valid for advection-dominated problems. In regions of a model domain where the grid Peclet number is less than about 1, the method produces inaccurate results. Finally, the matrix diffusion method is valid only if the solute has insufficient time to diffuse fully between fractures during the time scale of a simulation.

### 8.3.5 Numerical Method Type

For the reactive transport model, the approximation of the partial differential equations for solute transport parallels exactly the theory outlined for the solution of the flow and energy transport equations in Section 8.1.6. The concentrations of all solutes must be solved simultaneously, since the concentrations are coupled through the kinetic or equilibrium reaction terms. The code employs an option that we denote as selective coupling to solve multiple solute concentrations directly using the multiple degree-of-freedom equation solver. When more than four solutes

are present, an iterative procedure is required. This method is outlined in detail in Section 8.3.6.

The RTTF particle tracking method is a Lagrangian numerical method that employs transfer functions to compute particle residence times in each cell. Thus the time a particle spends in a cell, as well as the decision of which adjacent cell to travel to next, are determined probabilistically.

## 8.3.6 Derivation of Numerical Model

### 8.3.6.1 Reactive Transport Model

Since many aspects of the reactive transport numerical methods parallel the development of the fluid and energy transport numerical method, only the parts of the development that are unique to solute transport are outlined here. The reactive transport equations given by Equations (82), (83) and (84) result in a set of nonlinear coupled PDEs. The numerical implementation of the transport step can be derived by rewriting Equations (82), (83) and (84) in fully implicit time-discretized form:

$$\frac{C_j^{n+1} - C_j^n}{\Delta t} + L(C_j)^{n+1} = R_j^{n+1} \tag{106}$$

$$\frac{G_k^{n+1} - G_k^n}{\Delta t} + L(G_k)^{n+1} = R_k^{n+1} \tag{107}$$

$$\frac{M_m^{n+1} - M_m^n}{\Delta t} = R_m^{n+1} \tag{108}$$

where n indicates the time step level. Reactive transport codes in the literature solve equations (106), (107) and (108) using either the global implicit, operator splitting, or sequential iterative methods. The global implicit method solves the transport and reaction step simultaneously. On the other hand, operator splitting methods solve the transport and reaction steps in sequence without iteration. Finally, the sequential iterative approaches iterate between the transport and reaction steps until a fully implicit solution is achieved. In this paper, we present a technique which is a hybridized version of the global implicit and sequential iteration methods.

The reaction rate terms in equations (106), (107) and (108) can be estimated using a Taylor series expansion to linearize the reaction rate term

$$R_i^{n+1,\,p+1} = R_i^{n+1,\,p} + \sum_{j=1}^{N_c} \left(\frac{\partial R_i}{\partial C_j}\right)^{n+1,\,p} (C_j^{n+1,\,p+1} - C_j^{n+1,\,p}) +$$

$$\sum_{k=1}^{N_v} \left(\frac{\partial R_i}{\partial G_k}\right)^{n+1,\,p} (G_k^{n+1,\,p+1} - G_k^{n+1,\,p}) +$$

$$\sum_{m=1}^{N_{im}} \left(\frac{\partial R_i}{\partial M_m}\right)^{n+1,\,p} (M_m^{n+1,\,p+1} - M_m^{n+1,\,p}) + \ldots \qquad (109)$$

where p is the iteration level and i represents either an aqueous, vapor or immobile component.

The iterative methods in the literature differ in the number of terms evaluated in this Taylor series expansion. Expanding each term on the left hand side of equations (106), (107) and (108) in a Taylor series (neglecting the higher order Taylor series terms) and substituting the expanded reaction rate given by Equation (109) results in a set of linear algebraic equations which constitute a single iteration of the Newton-Raphson method. This fully coupled approach is called the global implicit method. However, the Newton-Raphson method results in a large system of coupled linear equations stemming from the derivative terms of $R_i$ with respect to other aqueous, vapor, or immobile components. The approximate iterative approaches in the reactive transport literature often drop terms in the Taylor series expansion to decouple the linear equations into smaller equations sets that are solved sequentially. The sequential iterative approach described by Engesgaard and Kipp(1992) and Kinzelbach et al.(1991) use only the first term in the Taylor series ($R_i^{n+1,\,p}$). We will refer to this method as the SIA-0 method. The SIA-1 method (Tebes-Stevens, et al.(1998)) estimates the reaction term as:

$$R_i^{n+1,\,p+1} = R_i^{n+1,\,p} + \left(\frac{\partial R_i}{\partial C_i}\right)^{n+1,\,p} (C_i^{n+1,\,p+1} - C_i^{n+1,\,p}) \qquad (110)$$

The SIA-1 approach seeks to improve the estimate of $R_i^{n+1,\,p+1}$ by considering the relationship between $R_i$ and $C_i$ only. That is, the relationships with other aqueous, vapor and immobile components are neglected, and the linear equations arising from the individual components are solved separately. We have found that the SIA-1 greatly improves convergence for large Damkohler number systems, when kinetics are fast compared to

the transport time scale (Tebes-Stevens et al.(1998)). SIA-1 often outperforms SIA-0 because the $\partial R_i/\partial C_j$ term is often significant, whereas, $\partial R_i/\partial C_j, i \neq j$ terms are not. However, for certain reactions, the SIA-1 approach becomes quite inefficient because some of the cross derivative terms ($\partial R_i/\partial C_j, i \neq j$) that are neglected by SIA-1 are significant. Physically, this can occur when aqueous, vapor, or immobile components that are, in fact, coupled to one another are treated as though they were independent.

**Selective Coupling and Coupled Normalization**

*Selective Coupling*: In an extension of the SIA methods, we selectively include additional derivative terms that couple a subset of the components to one another to improve convergence. We call this method “Selective Coupling” to denote the flexibility of the implementation. Since cross derivative terms, $\partial R_i/\partial C_j$, are now included in the calculation, sets of components must be solved simultaneously. We note in passing that in the extreme case in which only $\partial R_i/\partial C_i$ are calculated, the method reduces to the SIA-1 method. At the other extreme, in which all components are coupled, a global implicit solution scheme[16] is effectively obtained. The algorithm is best illustrated through specific examples. For this, we first consider the following reaction system of kinetic reactions among aqueous components:

$$A \Leftrightarrow B;\ R_A = k_{f1}C_A - k_{r1}C_B \tag{111}$$

$$B \Leftrightarrow C;\ R_B = k_{f2}C_B - k_{r2}C_C \tag{112}$$

$$C \Leftrightarrow D;\ R_C = k_{f3}C_C - k_{r3}C_D \tag{113}$$

We start with the fully coupled formulation of the transport problem. The equation set resulting from the use of Newton's method to solve the nonlinear system of equations is represented in block matrix form below:

$$\begin{bmatrix} a_{11} & t_{12} & & & & & \\ t_{21} & a_{22} & t_{23} & & & & \\ & t_{32} & a_{33} & t_{34} & & & \\ & & \cdot & \cdot & \cdot & & \\ & & & \cdot & \cdot & \cdot & \\ & & & & \cdot & \cdot & t_{N_N-1,N_N} \\ & & & & & t_{N_N,N_N-1} & a_{N_N N_N} \end{bmatrix} \begin{bmatrix} \delta C_1 \\ \delta C_2 \\ \delta C_3 \\ \cdot \\ \cdot \\ \cdot \\ \delta C_{N_N} \end{bmatrix} = \begin{bmatrix} f_1 \\ f_2 \\ f_3 \\ \cdot \\ \cdot \\ \cdot \\ f_{N_N} \end{bmatrix} \quad (114)$$

in which each element in the matrix is a $N_{dof} \times N_{dof}$ submatrix containing elements of the Jacobian matrix ($\partial f_i / \partial C_j$), $\delta C$ is the vector of change in component concentration at node i ($\delta C_A, \delta C_B, \delta C_C$ and $\delta C_D$), $N_N$ is the number of spatial nodes, and the $f_i$ are the residual arrays which contain the advection, dispersion, accumulation, and reaction terms (length of $N_{dof}$, where $N_{dof}$ is the number of "degrees of freedom," in this case equal to four, the number of components in the example). The elements of the Jacobian matrix contain derivatives of the residual with respect to concentration. In the diagram, a tri-diagonal matrix resulting from a one-dimensional transport problem is shown for simplicity, but is not a restriction of the method. For our example reactive transport system, the submatrix **a** and submatrix **t** at a node q connected to node q+1 are given by:

$$a = \begin{bmatrix} \frac{\partial f_A}{\partial C_A} & \frac{\partial f_A}{\partial C_B} & 0 & 0 \\ \frac{\partial f_B}{\partial C_A} & \frac{\partial f_B}{\partial C_B} & \frac{\partial f_B}{\partial C_C} & 0 \\ 0 & \frac{\partial f_C}{\partial C_B} & \frac{\partial f_C}{\partial C_C} & \frac{\partial f_C}{\partial C_D} \\ 0 & 0 & \frac{\partial f_D}{\partial C_C} & \frac{\partial f_D}{\partial C_D} \end{bmatrix}; \quad t = \begin{bmatrix} \frac{\partial f_A}{\partial C_{A,q+1}} & 0 & 0 & 0 \\ 0 & \frac{\partial f_B}{\partial C_{B,q+1}} & 0 & 0 \\ 0 & 0 & \frac{\partial f_C}{\partial C_{C,q+1}} & 0 \\ 0 & 0 & 0 & \frac{\partial f_D}{\partial C_{D,q+1}} \end{bmatrix} \quad (115)$$

where the **a** matrix is written at node q, and q+1 represents a node connected to node q. In general, the structure of submatrix **a** is defined by the reaction system. Now suppose that the reaction in equation (112) is slow compared to the other two

reactions. In the submatrix **a**, the terms $\partial f_B/\partial C_C$ and $\partial f_C/\partial C_B$ would be small compared to the other elements of **a**, and **a** can be approximately represented as:

$$a = \begin{bmatrix} \frac{\partial f_A}{\partial C_A} & \frac{\partial f_A}{\partial C_B} & 0 & 0 \\ \frac{\partial f_B}{\partial C_A} & \frac{\partial f_B}{\partial C_B} & 0 & 0 \\ 0 & 0 & \frac{\partial f_C}{\partial C_C} & \frac{\partial f_C}{\partial C_D} \\ 0 & 0 & \frac{\partial f_D}{\partial C_C} & \frac{\partial f_D}{\partial C_D} \end{bmatrix} \quad (116)$$

This system can then be solved in two steps, with the $A$ and $B$ equations solved simultaneously, followed by the $C$ and $D$ equations solved in a second step. A reactive transport computer code that employs this method allows the user to "selectively couple" the components in the transport iteration. The decomposition of a four-degree-of-freedom problem into two two-degrees-of-freedom problems results in memory efficiencies and computational savings per iteration, and therefore is a desirable alternative to a full global implicit solution for some applications. Note that when all off-diagonal terms in the submatrix **a** are omitted, each of the four components can be solved iteratively and sequentially, i.e. the SIA-1 method is obtained.

When more than one component is solved simultaneously, an equation solver that handle block matrices is required. The linear equation solver in FEHM, developed primarily for the solution of coupled fluid flow and heat transport, makes use of well-tested numerical techniques that take advantage of the block structure of the coupled equations for pressure, temperature, and fluid saturation. Here, we use the same solver technologies for the transport solution step. In essence, for $N_{dof}$ (where $N_{dof}$ unknowns per grid point, the same operations on the overall matrix of a single-unknown solution are carried out, but multiplications of individual matrix elements now become matrix multiplications involving the $N_{dof} \times N_{dof}$ submatrices, and divisions are carried out as multiplications by the inverse of the submatrix. Since such operations become memory and cpu intensive for large problems, it is important to employ efficient numerical techniques. FEHM uses numerical methods suitable for the

nonsymmetric matrices that arise from the finite element solution of reactive transport equations on unstructured numerical grids. The solver software uses incomplete factorization with variable fill-in level as a preconditioner, and a generalized minimum residual (GMRES) acceleration technique for the iterative solution. Details of this method as applied to heat and mass transport problems may be found in Zyvoloski et al.(1997). In a typical reactive transport solution with FEHM, the heat and mass transfer solution is also being performed, so the initial bookkeeping associated with the method is already being carried out, and the memory allocated for the solution is shared between the heat and mass solution and the transport solution.

There are definite trade-offs in computational efficiency and memory utilization between the SIA techniques and methods involving coupling of the transport equations of individual components. Coupling requires more time per iteration and more memory than typical SIA methods. However, components strongly coupled by reaction may not converge using SIA methods without using small time steps. Since flexibility is required in a general purpose code, the transport iteration in FEHM was developed with the Selective Coupling provision to solve the component concentrations in groups of one or more at a time, so that only those components that need to be coupled are solved simultaneously. It is necessary to solve a set of equations for each component present in the system, but the order of solution and the nature of the coupling are set by the user at run-time. This allows the user, on the basis of his knowledge of the reactive transport system, to couple only those components that are required for efficient solution of the system of equations. Selective Coupling of components linked to each other through kinetic chemical reactions allows a given problem to be solved in the fastest, yet most memory efficient manner possible.

*Coupled Normalization*: When residual equations are solved simultaneously, it is advisable to normalize them so that they are solved to the same degree of numerical precision. We now present a method we call “Coupled Normalization” for accomplishing this in a manner that in some cases has the added benefit of effectively reducing the number of degrees of freedom of the solution. Again, we will make use of an example to illustrate the method, in this case a kinetic ion exchange reaction of the form

$$A + B\text{-}X \Leftrightarrow B + A\text{-}X \tag{117}$$

$$R_A = k_f[A][B\text{-}X] - k_r[B][A\text{-}X] \tag{118}$$

This example consists of two aqueous components, which in general can undergo aqueous speciation reactions, though not in this example, and two immobile components. As in the previous

example, $N_{dof}$ is four because we will solve for these four components simultaneously. Furthermore, the block matrix equation set in (114) also applies here. The submatrices **a** and **t** are given by:

$$a = \begin{bmatrix} \frac{\partial f_A}{\partial C_A} & \frac{\partial f_A}{\partial C_B} & \frac{\partial f_A}{\partial M_{A\text{-}X}} & \frac{\partial f_A}{\partial M_{B\text{-}X}} \\ \frac{\partial f_B}{\partial C_A} & \frac{\partial f_B}{\partial C_B} & \frac{\partial f_B}{\partial M_{A\text{-}X}} & \frac{\partial f_B}{\partial M_{B\text{-}X}} \\ \frac{\partial f_{A\text{-}X}}{\partial C_A} & \frac{\partial f_{A\text{-}X}}{\partial C_B} & \frac{\partial f_{A\text{-}X}}{\partial M_{A\text{-}X}} & \frac{\partial f_{A\text{-}X}}{\partial M_{B\text{-}X}} \\ \frac{\partial f_{B\text{-}X}}{\partial C_A} & \frac{\partial f_{B\text{-}X}}{\partial C_B} & \frac{\partial f_{B\text{-}X}}{\partial M_{A\text{-}X}} & \frac{\partial f_{B\text{-}X}}{\partial M_{B\text{-}X}} \end{bmatrix} ; \; t = \begin{bmatrix} \frac{\partial f_A}{\partial C_{A,\,q+1}} & 0 & 0 & 0 \\ 0 & \frac{\partial f_B}{\partial C_{B,\,q+1}} & 0 & 0 \\ 0 & 0 & 0 & 0 \\ 0 & 0 & 0 & 0 \end{bmatrix} \quad (119)$$

The immobile components are not present in the **t** submatrices since there are no transport terms associated with them. Before solving the linear equation set, we apply the Coupled Normalization step, which consists of multiplying both sides of the equation set at each node by the inverse of **a**, which of course transforms each submatrix **a** into the identity matrix. This operation scales the diagonal term of each equation to the same value (unity), thereby normalizing the equation set to ensure that when a typical convergence criterion, such as one based on the L2 norm, is employed, each equation is solved to the same level of accuracy on a normalized basis. Coupled normalization serves another important function for systems with immobile components, as evidenced by the structure of the transport submatrix **t'** after multiplication by $\mathbf{a^{-1}}$

$$t' = \begin{bmatrix} X & X & 0 & 0 \\ X & X & 0 & 0 \\ X & X & 0 & 0 \\ X & X & 0 & 0 \end{bmatrix} \quad (120)$$

where the $X$ denotes a non-zero term. After coupled normalization, the mobile component equations no longer contain terms involving the immobile component unknowns in either the transformed submatrix a or the t' submatrix. Thus the first two equations can now be solved as a coupled two by two equation set for the concentration changes of the mobile species, after which the immobile component unknowns are then solved for individually by simple back-substitution. Coupled normalization in effect folds the cross derivative

information from the immobile component equations into the equations for the mobile components, so that only the two mobile component unknowns need be solved simultaneously. This method effectively reduces the number of degrees-of-freedom in the transport solution by the number of immobile components in the system of equations (two in this example), thereby reducing the memory utilization and computational burden of the solution.

#### 8.3.6.2 Particle Tracking Model

All aspects of the numerical model for particle tracking are discussed in Section 8.3.3.2.

### 8.3.7 Location

The implementation sequence for either the Reactive Transport Model or the Particle Tracking Model is illustrated in Fig. 1. The two models cannot be run simultaneously in the current version of FEHM. After a heat and mass transfer time step is taken and the flow and temperature fields are determined, the solute transport solution is computed from the previous heat and mass time to the current time. The flow field used for the transport calculations are assumed to be unchanging during this time.

### 8.3.8 Numerical Stability and Accuracy

**Reactive Transport Model.** As in the heat and mass transfer solution discussion (Section 8.1.8), nonlinearities can give rise to problems with stability of the solution. The formulation of the problem as a fully coupled, implicit solution maximizes the likelihood of obtaining a stable, accurate solution. Accuracy is also intimately tied to the grid discretization, time step, and dispersion coefficients of the solutes. Advection dominated transport with low dispersion coefficients is well known to be difficult to simulate accurately with finite difference or finite element techniques. Testing the solution against the results of a calculation with smaller grid spacings and time steps is one way to assess the level of numerical dispersion. Another way is to compare the solution to a particle tracking simulation, which is designed to minimize numerical inaccuracies.

**Particle Tracking Model.** The accuracy of a RTTF particle tracking should be evaluated using the following considerations:

- The dispersion coefficient must be set high enough to avoid grid Peclet numbers less than 1; in fact, the code sets the Peclet number of a cell to 1 for any value lower than 1.
- Diffusion into the rock matrix must be slow enough that the solute has insufficient time to diffuse fully to the centerline between fractures.
- If the velocity vectors are not aligned with the finite element grid, some inaccuracies due to grid orientation effects are to be expected.
- The number of particles in the simulation must be sufficient to minimize errors induced by statistical fluctuations.

### 8.3.9 Alternatives

**Reactive Transport Model.** Many different numerical formulations of the reactive transport problem are possible. A review of these methods was performed by Yeh and Tripathi (1989). These models differ in the number

of species that can be simulated, and the nature of the chemical reactions that can be simulated. When equilibrium is assumed for all reactions, the reaction part of the problem can effectively be decoupled from the transport, and considerable simplification results. For combined kinetic and equilibrium formulations, Friedly and Rubin (1992) have shown that similar simplifications are possible. Most models presented in the literature that use sophisticated chemical sub-models are restricted to simplified flow geometries and flow physics or require a flow solution as input, and the number of grid points that can practically be simulated is small.

The reactive transport model developed here was specifically designed for use in the context of large-scale two- and three-dimensional simulations. It was assumed that in the near future, computational resources would be insufficient to handle a large number of chemical species for a large-scale problem of many thousands of grid points. Therefore, the model development assumed that information from other sources (geochemical codes, literature data for a few key reactions and species) could be abstracted and distilled into a relatively small number of interacting solutes. Given this assumption, the logical method of solution was to utilize the multiple degree-of-freedom solution technology that is at the center of the FEHM code. Alternative techniques such as those referred to above will be evaluated and incorporated into future versions of FEHM, as needed.

**Particle Tracking Model.** The RTTF particle tracking modeling approach in FEHM differs from most groundwater particle tracking algorithms reported in the literature [e.g. Tompson and Gelhar (1990), Lu (1994)]. These methods require that the velocity vector be resolved accurately at each location in the model domain. This usually involves an interpolation method to obtain the velocity at any position needed based on the values computed from a flow simulation (at cell faces or nodes, for example). Then, the algorithm consists of marching forward in small time steps, computing the trajectory and new location of the particle at the new time. Equilibrium, linear sorption is modeled by introducing a retardation factor to reduce the particle velocity. Dispersion is handled using a random walk approach that displaces the particle a certain amount during each time step, so that the particle samples a different velocity field than it would have in the absence of dispersion.

By contrast, the approach used in the FEHM particle tracking algorithm uses the fluid mass fluxes from node to node as the basis for moving particles. These are the quantities that are actually known in integrated finite difference and finite element calculations, while the velocity vectors are interpolated results. Thus the implementation of the RTTF technique in an existing code like FEHM is straightforward. Another practical advantage is that the computations are extremely fast: simulations with several million particles are practical using conventional workstations. One compromise in the approach is the limitation to advection dominated transport systems. This was thought to be a reasonable compromise, especially in the context of a code that already has a reactive transport module that easily handles systems with high dispersion coefficients.

## 8.4 Constitutive Relationships

### 8.4.1 Purpose

The densities, viscosities, and enthalpies of water, water vapor, and air are required for the simulation of the Flow and Transport in a porous medium. These constitutive relations depend on temperature and pressure. To be computationally efficient, the form of these relations must be easy to compute and accurate. To satisfy these needs rational polynomial fits to the National Bureau of Standards Steam Tables are used. The models require the pressure and temperature of a node as input and output the densities, viscosities, and enthalpies of the phases.

### 8.4.2 Assumptions and Limitations

At present, several fits of the data are available to the user. These allow usage of the relations for temperatures up to 360 °C and pressures up to 110 MPa. If the variable exceeds the limits of the data, the FEHM code will restart the timestep with a smaller time step size and try to keep the variable within the bounds of the data.

### 8.4.3 Derivation

**Pressure and Temperature Dependent Fluid Properties**. A porous flow simulator, such as FEHM, with heat and mass transfer capabilities requires the functional dependence of the phase densities, the phase enthalpies, and the phase viscosities on temperature ($T$) and pressure ($P$). Because FEHM is an implicit code which uses a Newton-Raphson iteration, derivatives of the thermodynamic functions with respect to $P$ and $T$ are also required.

Rational function approximations are used to estimate the thermodynamic variables in FEHM where the rational functions are a ratio of polynomials. Complete polynomials of order three are used in both the numerator and denominator. For example, the density is approximated as

$$\rho(P, T) = \frac{Y(P, T)}{Z(P, T)} \tag{121}$$

where

$$Y(P, T) = Y_0 + Y_1 P + Y_2 P^2 + Y_3 P^3 + Y_4 T + Y_5 T^2 + Y_6 T^3 + Y_7 PT + Y_8 P^2 T + Y_9 PT^2 \tag{122}$$

and

$$Z(P, T) = Z_0 + Z_1 P + Z_2 P^2 + Z_3 P^3 + Z_4 T + Z_5 T^2 + Z_6 T^3 + Z_7 PT + Z_8 P^2 T + Z_9 PT^2 . \tag{123}$$

This type of relationship has been shown by Zyvoloski and Dash (1991) to provide an accurate method for determining parameter values over a wide

range of pressures and temperatures, as well as allowing derivatives with respect to pressure and temperature to be computed easily.

Polynomial coefficients were obtained by fitting data from the National Bureau of Standards OSRD database 10, the database used for the *NBS/NRC Steam Tables* (Harr, et al. 1984). The data fits result in errors less than one percent and often less than 0.1 percent. The coefficients used in FEHM are valid over the pressure and temperature ranges $0.001 \le P \le 110.0$ MPa and $0.001 \le T \le 360$ °C. Polynomial coefficients for the enthalpy, density, and viscosity functions are given in Table III of the Appendix.

**Pressure as a function of saturation temperature / Temperature as a function of saturation pressure**. The equation for the saturation line is important for the determination of the phase state of the liquid vapor system. The saturation line may be described in a water only system as the pressure above which boiling occurs. In a mixture of air or other noncondensible gas, the saturation line is simply the partial pressure of water or the vapor pressure of water. Rational function approximations are also used for the saturation line equations:

$$P_v(T) = \frac{Y(T)}{Z(T)},\ T(P_v) = \frac{Y(P_v)}{Z(P_v)} \tag{124}$$

where

$$Y(X) = Y_0 + Y_1X + Y_2X^2 + Y_3X^3 + Y_4X^4 \tag{125}$$

and

$$Z(X) = Z_0 + Z_1X + Z_2X^2 + Z_3X^3 + Z_4X^4. \tag{126}$$

X represents temperature or pressure in the respective relationships. Polynomial coefficients for the saturation functions are given in Table IV of the Appendix.

FEHM also allows for the inclusion of a vapor pressure lowering term which may be important in situations where high capillary forces are present. The modified vapor pressure (Case, 1994) is given by:

$$P_v^*(T, P_{cap}) = P_v(T)\exp\left(\frac{-P_{cap}}{\rho_l R^*(T + 273.15)}\right) \tag{127}$$

where $P_v^*$ is the new vapor pressure of water, $P_{cap}$ is the capillary pressure, and $R^*$ is the gas constant divided by the molecular weight of water.

**Properties of Air and Air/Vapor Mixtures**. Appropriate thermodynamic information for air and air/vapor mixtures are provided. The density of air

is assumed to obey the ideal gas law. Using atmospheric conditions as the reference state

$$\rho_a = 1.292864\left(\frac{273.15}{T + 273.15}\right)\left(\frac{P_a}{0.101325}\right) \quad (128)$$

where $\rho_a$ has the units kg/m$^3$, $T$ is in °C, and $P$ is in MPa. The mixture density is given by

$$\rho_v = \rho_{v,w} + \rho_a \quad (129)$$

where $\rho_{v,w}$ is the density of water vapor.

The enthalpy of air is specified as a function of temperature only

$$h_a = c_{pa}(T \cdot 10^{-6}) \quad (130)$$

where

$$c_{pa} = 1003.7 + 0.025656T + 0.00045457T^2 - 2.7107 \times 10^{-7}T^3, \quad (131)$$

$h_a$ is the enthalpy of air (MJ/kg), and $c_{pa}$ is the heat capacity of air (MJ/kg °C). The parameters in Equation (131) were obtained by regression of a more complex correlation found in Sychev, et al. (1988). The mixture enthalpy for the vapor phase is

$$h_v = h_{v,w}(1 - \eta_v) + h_a\eta_v \quad (132)$$

where $h_{v,w}$ is the enthalpy of steam and $\eta_v$ is the fraction by mass of air in the vapor phase. The mixture enthalpy of the liquid phase is given by:

$$h_l = h_{l,w}(1 - \eta_l) + h_a\eta_l \quad (133)$$

where $h_{l,w}$ is the enthalpy of liquid water and $\eta_l$ is the mass fraction of air in the liquid phase.

Assuming ideal gas behavior, the mass fraction of air in the vapor phase may be expressed as

$$\eta_v = \frac{\rho_a}{\rho_v}. \quad (134)$$

The mass fraction of air in the liquid phase is assumed to obey Henry's law or

$$\eta_l = K_{H,a}P_a \quad (135)$$

where $K_{H,a}$ is the Henry's law constant for air ($K_{H,a}$ = 1.611 x $10^{-4}$ $Pa^{-1}$) and $P_a$ is the partial pressure of air.

The viscosity of the vapor phase is assumed to be a linear combination of the air viscosity and the water viscosity

$$\mu_v = \mu_{v,w}(1-\eta_v) + \mu_a \eta_v \tag{136}$$

where $\mu_{v,w}$ is the steam viscosity and is obtained from steam data. The viscosity of air is assumed constant

$$\mu_a = 1.82 \times 10^{-5} \ \frac{\mathrm{N \cdot s}}{\mathrm{m}^2}. \tag{137}$$

The liquid phase viscosity is assumed to be independent of the amount of dissolved air and is obtained from a rational function approximation like those specified above.

**Relative Permeability and Capillary Pressure Functions**. Relative permeabilities and capillary pressures can be strong functions of saturation. Several well known relative permeability functions are available to the user. They are the simple linear functions, the Corey (1954) relationships, and the van Genuchten (1980) functions. Composite relative permeability curves, as described by Klavetter and Peters (1986), are also a user option.

The linear functions are given by

$$R_l = \begin{cases} 0, & S_l \le S_{lr} \\ \dfrac{S_l - S_{lr}}{S_{lmax} - S_{lr}}, & S_{lr} < S_l < S_{lmax} \\ 1, & S_l \ge S_{lmax} \end{cases} \tag{138}$$

$$R_v = \begin{cases} 0, & S_v \le S_{vr} \\ \dfrac{S_v - S_{vr}}{S_{vmax} - S_{vr}}, & S_{vr} < S_v < S_{vmax} \\ 1, & S_v \ge S_{vmax} \end{cases} \tag{139}$$

where $S_{lr}$ is residual liquid saturation, $S_{vr}$ is residual vapor saturation, $S_{lmax}$ is maximum liquid saturation, and $S_{vmax}$ is maximum vapor saturation.

The Corey relative permeability functions are given by

$$R_l = \hat{S}_l^4, \tag{140}$$

$$R_v = (1-\hat{S}_l)^2(1-\hat{S}_l^2) \tag{141}$$

where $\hat{S}_l = \dfrac{S_l - S_{lr} - S_{vr}}{1 - S_{lr} - S_{vr}}$ and $S_{lr}$ and $S_{vr}$ are the residual liquid and vapor saturations respectively.

The van Genuchten relative permeability functions are described by the following formulae:

$$R_l = \begin{cases} \left[1.0 - \left(1.0 - \hat{S}^{\frac{1}{\lambda}}\right)^{\lambda}\right]^2 \sqrt{\hat{S}}, & \hat{S} < S_{lmax} \\ 1.0, & \hat{S} \geq S_{lmax} \end{cases} \tag{142}$$

$$R_v = 1.0 - R_l \tag{143}$$

where $\hat{S} = \dfrac{S_l - S_{lr}}{S_{lmax} - S_{lr}}$ and $\lambda = 1 - \dfrac{1}{n}$, where $n$ is an experimentally determined parameter.

$R_l$ and $R_v$ are restricted by the requirement that $0.0 \leq R_l \leq 1.0$ and $0.0 \leq R_v \leq 1.0$. The relative permeability functions are truncated to the appropriate value if the these conditions are violated.

The capillary functions considered are the linear function and the van Genuchten capillary pressure model. Our terminology follows that of Pruess (1991).

The linear capillary function model is given by the following equations

$$P_{cap} = \begin{cases} P_{capmax}, & S_l \leq S_{lr} \\ P_{capmax}\dfrac{S_{lmax} - S_l}{S_{lmax} - S_{lr}}, & S_{lr} < S_l < S_{lmax} \\ 0.0, & S_l \geq S_{lmax} \end{cases} \tag{144}$$

where $P_{capmax}$ is the maximum capillary pressure, $S_{lr}$ is the residual liquid saturation, and $S_{lmax}$ is the maximum liquid saturation. The restriction $S_{lmax} > S_{lr}$ is also necessary.

The van Genuchten functions (van Genuchten, 1980) for capillary pressure are described by the following equations

$$P_{cap} = \begin{cases} P_{capmax}, & P_{cap1} \geq P_{capmax} \\ P_{cap1}, & P_{cap1} < P_{capmax} \\ 0.0\ , & S_l \geq S_{lmax} \end{cases} \tag{145}$$

where $P_{cap1} = P_0\left[\hat{S}^{-\frac{1}{\lambda}} - 1.0\right]^{1.0-\lambda}$, $\hat{S} = \frac{S_l - S_{lr}}{S_{lmax} - S_{lr}}$, $P_0 = \frac{1.0}{\alpha_G}$, and $\lambda = 1 - \frac{1}{n}$ ($n$ and $\alpha_G$ are experimentally determined parameters).

The van Genuchten capillary pressure curves approach an infinite value as $S_l$ approaches 0 and 1. This requires the use of extrapolation techniques. At low saturations both linear and cubic fits are available. At high saturations a linear fit is used.

It should be noted that the van Genuchten relative permeability functions can be formulated in terms of capillary pressure by combining equations (142) and (145). While this may seem equivalent to the saturation based equation (142), some differences occur at very high or very low saturations. As mentioned previously, linear extensions of the capillary pressure and relative permeability functions are required in these regions. If a capillary pressure formulation of the relative permeability is used, then no separate linear extrapolation is needed for the relative permeability model as the capillary pressure is constrained to realistic values through its own extrapolation fits at low and high saturations. It should also be noted that a different relative permeability is sometimes used for the air phase:

$$R_v = \begin{cases} \left[\left(1.0 - \hat{S}^{\frac{1}{\lambda}}\right)\right]^{2\lambda} \sqrt{1-\hat{S}}, & \hat{S} < S_{lmax} \\ 0.0, & \hat{S} \geq S_{lmax} \end{cases} \qquad (146)$$

This replaces equation (143) in some models.

**Stress Dependent Properties**. Often it is necessary to accommodate changes in the rock porosity and permeability due to changes in effective stress caused by temperature and pore fluid pressure changes. A linear and nonlinear model are incorporated in the code for this purpose.

The linear pore pressure model for porosity is given by

$$\phi = \phi_0 + \alpha_a(P - P_0) \qquad (147)$$

where $\phi$ is the porosity at pressure $P$, $\phi_0$ is the porosity at pressure $P_0$, $\alpha_a$ is the aquifer compressibility.

The nonlinear model of fracture porosity (Gangi, 1978, Appendix) is given by

$$\phi = \phi_0\left[1 - \left(\frac{P_c}{P_x}\right)^m\right] \qquad (148)$$

and

$$P_c = \sigma - P - \alpha E \Delta T \tag{149}$$

where $P_c$ is the closure stress, $\sigma$ is the *in situ* stress (assumed isotropic), $\alpha$ is the coefficient of thermal expansion of the rock, $E$ is Young's modulus, $\Delta T$ is the temperature change of the rock, and $P_x$ and $m$ are parameters in the model.

For the Gangi Model the effect of stress and temperature changes on permeability are modeled with

$$k = k_0 \left( \frac{\phi}{\phi_0} \right)^3 \tag{150}$$

where $k_0$ is the permeability at porosity $\phi_0$.

**Variable Thermal Conductivity.** The thermal conductivity of the solid is often more accurately characterized as a function of temperature or liquid saturation. A linear temperature-dependent model and a relation based upon the square root of liquid saturation are incorporated in the code for this reason.

The linear temperature dependent model is given by

$$K_T = K_{ref} + K_s (T - T_{ref}) \tag{151}$$

where $K_T$ is the temperature dependent thermal conductiivity, $K_{ref}$ is the thermal conductivity at the reference temperature $T_{ref}$, and $K_s$ is the slope of the linear relation.

The saturation dependent thermal conductivity model is given by

$$K_{sat} = K_{dry} + K_{s,s} \sqrt{S} \tag{152}$$

where $K_{sat}$ is the saturation dependent thermal conductivity, $K_{dry}$ is the conductivity at 0 saturation, and $K_{s,s}$ is the slope of the linear relationship. Note that the conductivity at complete saturation is $K_{dry} + K_{s,s}$.

### 8.4.4 Application

The Constitutive Relationships discussed in Section 8.4 describe parameters that are used in the models described in previous sections. The discussion provided in Section 8.1.4 is also applicable here.

### 8.4.5 Numerical Method Type

The Newton Raphson method is used to calculate saturation and temperature as a function of pressure. The method has been previously described in Section 8.1.6.

### 8.4.6 Derivation of Numerical Model

The relative permeability and capillary functions represent the most nonlinear parts of FEHM and special consideration has been given them. A procedure similar to that used by Nitao (1988) is used to restrict the van Genuchten capillary function, Equation (145), to finite values when approaching zero saturation. The procedure is simple. At a low saturation, usually input by the user, the van Genuchten functions are replaced with linear fits that match the van Genuchten function at the specified saturation value and attain a maximum value, usually twice the value at the specified saturation, at zero saturation. This new capillary pressure is then used in the calculation of the relative permeability. The formulation in FEHM differs from Nitao's implementation in that it uses a cubic spline fit to match both the value and the slope at the specified saturation. At zero saturation the coefficients of the spline are adjusted so a zero slope and a zero second derivative is achieved. This assures a monatomically increasing function for the capillary pressure.

### 8.4.7 Location

The constitutive relationships are used to obtain the parameters that define the Flow and Energy Transport Equations. Referring to Fig. 1, the box labeled 'Get thermodynamic parameters' represents calls to routines that form the constitutive relationships.

### 8.4.8 Numerical Stability and Accuracy

The formulation of the constitutive relationship is directly related to the overall accuracy of the FEHM application. The accurate formulation of the water properties described in Section 8.4.3 was motivated by the need to have accuracy combined with computability. The discussion in Section 8.4.6 showed the need to have continuous and finite values of the constitutive functions. The authors believe there is still much work to be done in the area of extending the range of the functions as well as finding representations that will allow better convergence of the Newton Raphson iteration.

### 8.4.9 Alternatives

FEHM uses analytic derivatives of the constitutive relationships described in Section 8.4. The TOUGH code described by Pruess (1991) and the variant of TOUGH used by Nitao (1988) use numerical differences of the fluid and energy balance equations in the Newton Raphson iteration. Both of the methods have merit. The numerical derivative approach allows for possibly faster incorporation of new fluid physics models while the analytic derivative approach uses fewer iterations on tested problems (Reeves, 1993).

The functional representation of the constitutive models could be replaced by a tabular formulation. Several available codes have used tabular input for capillary and relative permeability data. FEHM will also incorporate tabular representations in future versions.

## 9.0 EXPERIENCE

The FEHM computer code and its predecessors have been used on a wide variety of problems ranging from geothermal to environmental remediation to radioactive

transport. When used in conjunction with its available grid generation package and post processing tools it has been a successful tool for modeling very complex geological settings and coupled fluid processes. When benchmarked against other codes it has been shown to be extremely competitive (Reeves, 1993).

**Table III. Polynomial Coefficients for Enthalpy, Density and Viscosity Functions**

| | | Enthalpy | | Density | | Viscosity | |
|---|---|---|---|---|---|---|---|
| | | Liquid | Vapor | Liquid | Vapor | Liquid | Vapor |
| Coefficients of Numerator | $Y_0$ | 0.25623465e-03 | 0.31290881e+00 | 0.10000000e+01 | 0.15089524e-05 | 0.17409149e-02 | -0.13920783e-03 |
| | $Y_1$ | 0.10184405e-02 | -0.10000000e+01 | 0.17472599e-01 | 0.10000000e+01 | 0.18894882e-04 | 0.98434337e-02 |
| | $Y_2$ | 0.22554970e-04 | 0.25748596e-01 | -0.20443098e-04 | -0.10000000e+01 | -0.66439332e-07 | -0.51504232e-03 |
| | $Y_3$ | 0.34836663e-07 | 0.38846142e-03 | -0.17442012e-06 | -0.16676705e-02 | -0.23122388e-09 | 0.62554603e-04 |
| | $Y_4$ | 0.41769866e-02 | 0.11319298e-01 | 0.49564109e-02 | 0.40111210e-07 | -0.31534914e-05 | 0.27105772e-04 |
| | $Y_5$ | -0.21244879e-04 | 0.20966376e-04 | -0.40757664e-04 | 0.25625316e-10 | 0.11120716e-07 | 0.84981906e-05 |
| | $Y_6$ | 0.25493516e-07 | 0.74228083e-08 | 0.50676664e-07 | -0.40479650e-12 | -0.48576020e-10 | 0.34539757e-07 |
| | $Y_7$ | 0.89557885e-04 | 0.19206133e-02 | 0.50330978e-04 | 0.43379623e-01 | 0.28006861e-07 | -0.25524682e-03 |
| | $Y_8$ | 0.10855046e-06 | -0.10372453e-03 | 0.33914814e-06 | 0.24991800e-02 | 0.23225035e-09 | 0.00000000e+00 |
| | $Y_9$ | -0.21720560e-06 | 0.59104245e-07 | -0.18383009e-06 | -0.94755043e-04 | 0.47180171e-10 | 0.12316788e-05 |
| Coefficients of Denominator | $Z_0$ | 0.10000000e+01 | 0.12511319e+00 | 0.10009476e-02 | 0.12636224e+00 | 0.10000000e+01 | 0.10000000e+01 |
| | $Z_1$ | 0.23513278e-01 | -0.36061317e+00 | 0.16812589e-04 | -0.30463489e+00 | 0.10523153e-01 | 0.10000000e+01 |
| | $Z_2$ | 0.48716386e-04 | 0.58668929e-02 | -0.24582622e-07 | 0.27981880e-02 | -0.22658391e-05 | -0.10000000e+01 |
| | $Z_3$ | -0.19935046e-08 | 0.99059715e-04 | -0.17014984e-09 | 0.51132337e-05 | -0.31796607e-06 | -0.10000000e+01 |
| | $Z_4$ | -0.50770309e-02 | 0.44331611e-02 | 0.48841156e-05 | 0.59318010e-02 | 0.29869141e-01 | 0.10000000e+01 |
| | $Z_5$ | 0.57780287e-05 | 0.50902084e-05 | -0.32967985e-07 | 0.80972509e-05 | 0.21844248e-03 | 0.10000000e+01 |
| | $Z_6$ | 0.90972916e-09 | -0.10812602e-08 | 0.28619380e-10 | -0.43798358e-07 | -0.87658855e-06 | -0.22934622e-03 |
| | $Z_7$ | -0.58981537e-04 | 0.90918809e-03 | 0.53249055e-07 | 0.53046787e-03 | 0.41690362e-03 | 0.10000000e+01 |
| | $Z_8$ | -0.12990752e-07 | -0.26960555e-04 | 0.30456698e-09 | -0.84916607e-05 | -0.25147022e-05 | 0.00000000e+00 |
| | $Z_9$ | 0.45872518e-08 | -0.36454880e-06 | -0.12221899e-09 | 0.48444919e-06 | 0.22144660e-05 | 0.25834551e-01 |
| Pressure range | | 0.001 - 110 MPa | 0.001 - 20 MPa | 0.001 - 110 MPa | 0.001 - 20 MPa | 0.001 - 110 MPa | 0.001 - 20 MPa |
| Temperature range | | 15 - 360°C | 15 - 360°C | 15 - 360°C | 15 - 360°C | 15 - 360°C | 15 - 360°C |

**Table IV. Polynomial Coefficients for Saturation Functions**

| | | Pressure | Temperature |
|---|---|---|---|
| Coefficients of Numerator | $Y_0$ | 0.71725602e-03 | -0.25048121e-05 |
| | $Y_1$ | 0.22607516e-04 | 0.45249584e-02 |
| | $Y_2$ | 0.26178556e-05 | 0.33551528e+00 |
| | $Y_3$ | -0.10516335e-07 | 0.10000000e+01 |
| | $Y_4$ | 0.63167028e-09 | 0.12254786e+00 |
| Coefficients of Denominator | $Z_0$ | 0.10000000e+01 | 0.20889841e-06 |
| | $Z_1$ | -0.22460012e-02 | 0.11587544e-03 |
| | $Z_2$ | 0.30234492e-05 | 0.31934455e-02 |
| | $Z_3$ | -0.32466525e-09 | 0.45538151e-02 |
| | $Z_4$ | 0.0 | 0.23756593e-03 |
| Pressure range | | 0.00123 - 14.59410 MPa | |
| Temperature range | | 10 - 340$^{\circ}$C | |